

Three-Dimensional Architecture of Ancient Lower Delta-Plain Point Bars Using Ground-Penetrating Radar, Cretaceous Ferron Sandstone, Utah

Rucsandra M. Corbeanu¹, Michael C. Wizevich², Janok P. Bhattacharya³,
Xiaoxiang Zeng³, and George A. McMechan³

ABSTRACT

Accurate three-dimensional description of reservoir architecture using outcrop analogs is hampered by limited exposure of essentially two-dimensional outcrops. This study contains the first fully three-dimensional description of ancient marine-influenced point bar sandstones of lower delta-plain distributary channels and is based on the integration of detailed outcrop and drill-hole data, and two- and three-dimensional ground-penetrating radar data. The studied outcrops are in the Cretaceous Ferron Sandstone of east-central Utah.

Point bars deposited in marine-influenced, lower delta-plain channels show complex facies and geometries that resemble both fluvial point bars (upward-fining grain-size distribution and laterally stacked inclined bedsets), and tidally influenced point bars (extensive mud drapes on the inclined bedset surfaces and upstream migration of inclined bedsets).

The bankfull width and mean bankfull depth were estimated at 225-150 m (738-492 ft) and at 3.9-5.2 m (12.8-17.1 ft), respectively. The heterogeneities in these point-bar deposits include mudstone drapes on the upper bounding surfaces of the inclined bedsets, and mudstone intraclast conglomerates lying on basal erosional scours of inclined bedsets. The spatial distribution of these heterogeneities is determined by direct mapping in outcrop in conjunction with modeling ground-penetrating radar amplitudes by geostatistical techniques. Mudstone layers are generally 5 m (16 ft) in length in the direction parallel to flow with a small percentage of mudstone layers 15 m (49 ft) in length, and 10 m (33 ft) perpendicular to flow, downdip along the inclined beds. The detailed distribution of heterogeneities inside reservoirs potentially affects flow behaviour.

¹Petrom SA, Campina, Romania; ²Department of Earth and Atmospheric Sciences, Cornell University, Ithaca, New York;

³Geosciences Department, University of Texas at Dallas, Richardson, Texas

INTRODUCTION

The three-dimensional (3-D) geometry of ancient point-bar deposits, either in alluvial or coastal channels is not known directly, but is usually inferred from two-dimensional (2-D) outcrops (Puigdefabregas and van Vliet, 1978; Flint and Bryant, 1993) combined with drill-hole data behind the outcrops (Van Wagoner et al., 1990; Falkner and Fielding, 1993). Rarely, two or more outcrops are oriented in orthogonal directions, yielding a pseudo 3-D view of the deposits. Three-dimensional geometry of point-bar deposits is better described in modern rivers deposits than in ancient deposits, but modern river deposits cannot be mapped below the water table, and lack complete documentation of the deposition over large time and space scales typical of outcrop examples. Studies of modern rivers also lack information about what is ultimately preserved in ancient deposits (Jackson, 1976; Bridge, 1985, 1993; Bridge et al., 1995). Theoretical models are used to predict variation in 3-D geometry of point bars under different conditions of channel migration (Bridge, 1984; Willis, 1989, 1993). However, these models are commonly simplified and cannot account for all parameters involved in the development of a point bar (e.g. the variable flow parameters, styles of migration, sediment load) and do not consider marine-influenced channels. New methods are needed to test inferred or theoretical point-bar models with real 3-D examples.

In this study we use 3-D ground-penetrating radar (GPR), to describe the 3-D internal structure of an ancient point-bar sandstone. Two-dimensional GPR surveys have been used in both modern unconsolidated sediments (Gawthorpe et al., 1993; Alexander et al., 1994; Bridge et al., 1995, 1998; Bristow et al., 2000) and ancient consolidated sedimentary rocks (Baker and Monash, 1991; Stephens, 1994; Bristow, 1995) to investigate the internal structure of sedimentary deposits, but true 3-D GPR studies are few (Beres et al., 1995; McMechan et al., 1997; Hornung and Aigner, 2000; Corbeau et al., 2001).

This study presents a detailed 3-D description of marine-influenced point-bar deposits of lower delta-plain distributary channels from the Ferron Sandstone Member of the Upper Cretaceous Mancos Shale in east-central Utah, by integrating detailed outcrop and drill-hole sedimentologic data with 100 MHz 2-D and 3-D GPR data. Published examples of point-bar deposits in deltaic distributary channels are all 2-D studies and refer especially to upper delta-plain channels (Elliott, 1976; Cherven, 1978; Hobday, 1978; Plint, 1983; Fielding, 1984; Hopkins, 1985).

Generally it is thought that lower delta-plain distributary channels are rather stable, do not migrate, and do not form point-bar or meander-belt deposits (Coleman and Prior, 1982, p. 155). Most fluvial point-bar

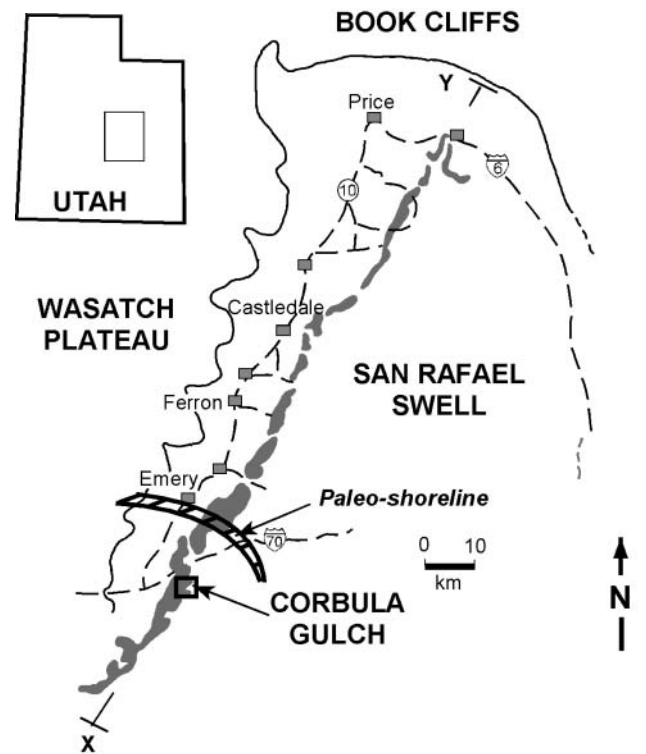


Figure 1. Location of the Corbula Gulch site in the Ferron Sandstone outcrop belt (the shaded area) along the southwestern flank of the San Rafael Swell in east-central Utah. X-Y represents the location of stratigraphic cross section in Figure 2. Paleo-shoreline during deposition of SC7 cycle is represented by hatched area.

models assume an upward overall decrease in mean grain size (from lag gravel and intraclast conglomerate, to sand and mud) and of the scale of the sedimentary structures, and a downstream decrease in grain size (Allen, 1964, 1970). In reality, fluvial point-bar deposits show more complexity than most idealized models (Jackson, 1976, 1978). Also, in relatively low-energy streams with significant suspended sediment load (Jackson, 1981), or in streams with minor tidal influence, muddy layers may drape point-bar surfaces, especially in the upper part of a point bar (Smith, 1987; Jordan and Pryor, 1992). In this paper we show that point bars deposited in marine-influenced, lower delta-plain channels show complex facies and geometries that share features of both fluvial- and tidal-point bars.

REGIONAL SETTING

Ferron Sandstone Stratigraphic Setting

The study area is located at Corbula Gulch along the western flank of the San Rafael Swell in east-central Utah. The outcrop is in the upper portion of the Ferron Sandstone known as the "Last Chance Delta" (Hale, 1972; Garrison et al., 1997) (Figure 1). The Ferron Sandstone Member is one of several clastic wedges that

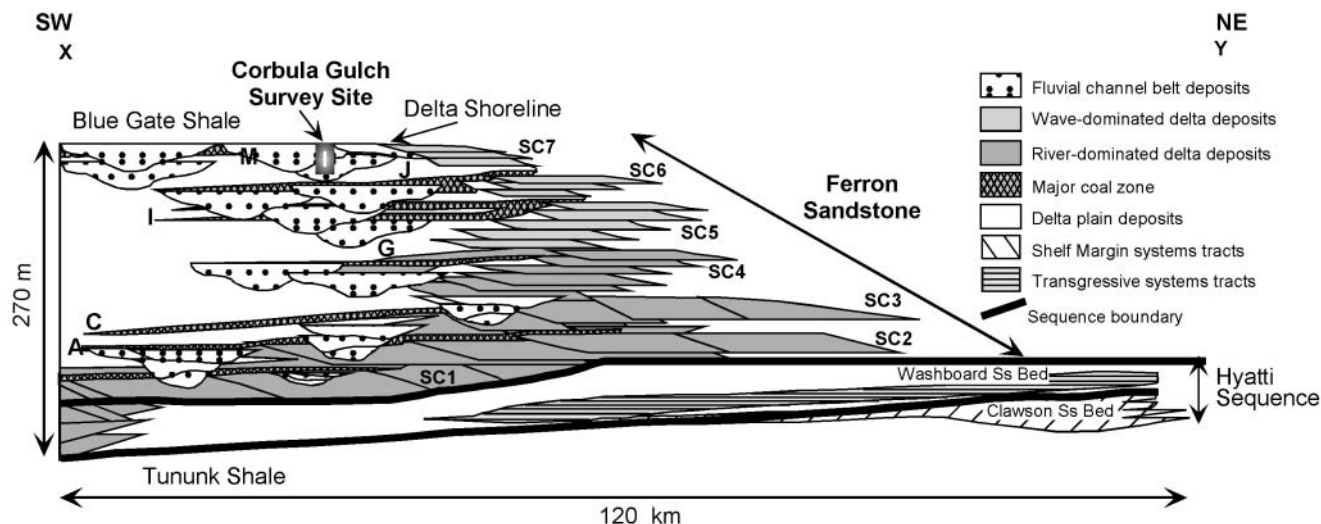


Figure 2. Generalized cross section of the upper part of the Ferron Sandstone clastic wedge (after Gardner, 1995). Stratigraphic location of survey site at Corbula Gulch and the paleo-shoreline are illustrated. See Figure 1 for location of cross section. Letters A to M identify major coal zones; SC1 to SC7 are short-term stratigraphic cycles.

prograded from the uplifted Sevier orogenic thrust belt northeast into the Mancos Sea during Turonian time (Hale, 1972; Cotter, 1975; Ryer, 1981; Gardner, 1992). The upper portion of the Ferron Sandstone is a deltaic complex that Ryer (1981, 1991) subdivided into seven deltaic cycles. Gardner (1992, 1995) defined the Ferron delta complex as a Type-2, third-order depositional sequence and also divided it into seven stratigraphic cycles, SC1 through SC7 (Figure 2). These cycles were also defined as parasequence sets by Ryer and Anderson (1995) and Garrison et al. (1997).

Gardner (1995) described facies tracts in successive short-term cycles, SC1 to SC3, as progradational, formed during an intermediate-term relative sea-level fall. Facies tracts of cycles SC4 and SC5 are aggradational and formed during a slow relative sea-level rise. Facies tracts of short-term stratigraphic cycles SC6 and SC7 are landward stepping and interpreted to be formed during a rapid relative sea-level rise. Each short-term cycle is capped by a major coal zone (Figure 2).

Corbula Gulch Stratigraphic Setting

The channel complex studied at Corbula Gulch is 12-15 m (39-49 ft) thick and consists of four erosively based, stacked channel bars within cycle SC7 (Figure 2). During cycle SC7 the coastline lay 24 km (15 mi) northeast of Corbula Gulch and became more embayed and influenced by marine conditions than the progradational cycles (SC1 to SC3) (cf. Ryer, 1991; Ryer and Anderson, 1995; Garrison et al., 1997) (Figure 1). The base of cycle SC7 rests on the J major coal zone that caps cycle SC6 (Garrison et al., 1997) and contains fine deposits composed of carbonaceous mudstones, fissile shales, dark-gray mudstones, coals, and small-scale cross-stratified, fine-grained sandstones with root traces (Figures 3 and

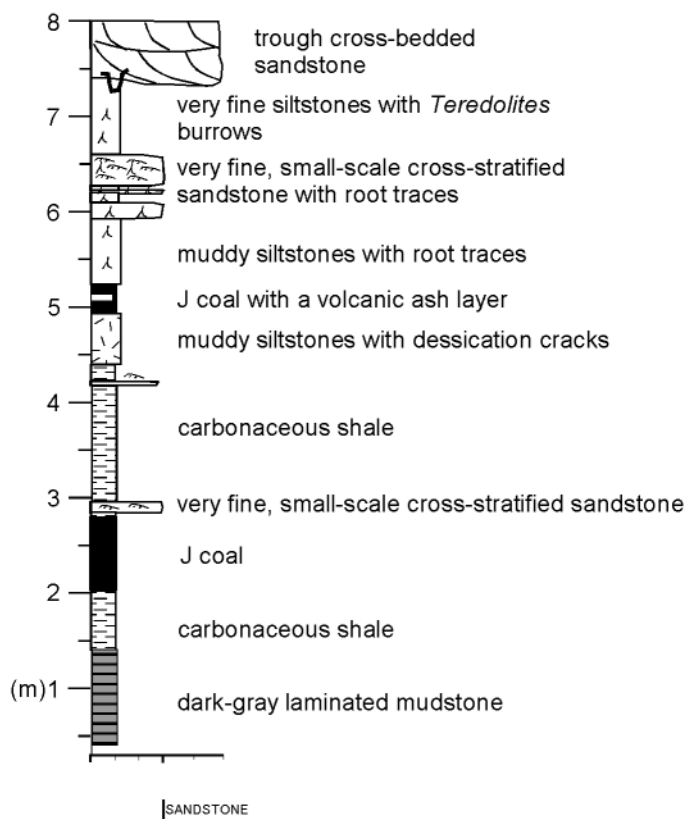


Figure 3. Generalized vertical measured section through the lower delta-plain deposits that underline the sandstone deposits. Vertical scale is in meters.

4A). In some locations, the uppermost coal bed contains a 15-cm-thick (6-in.) volcanic ash layer (Figure 4A). The muddy siltstone deposits contain desiccation cracks, abundant root traces (Figure 4B), and *Teredolites* burrows (Figure 4C). This combination of elements indicates immature paleosols and suggests a humid depositional environment.

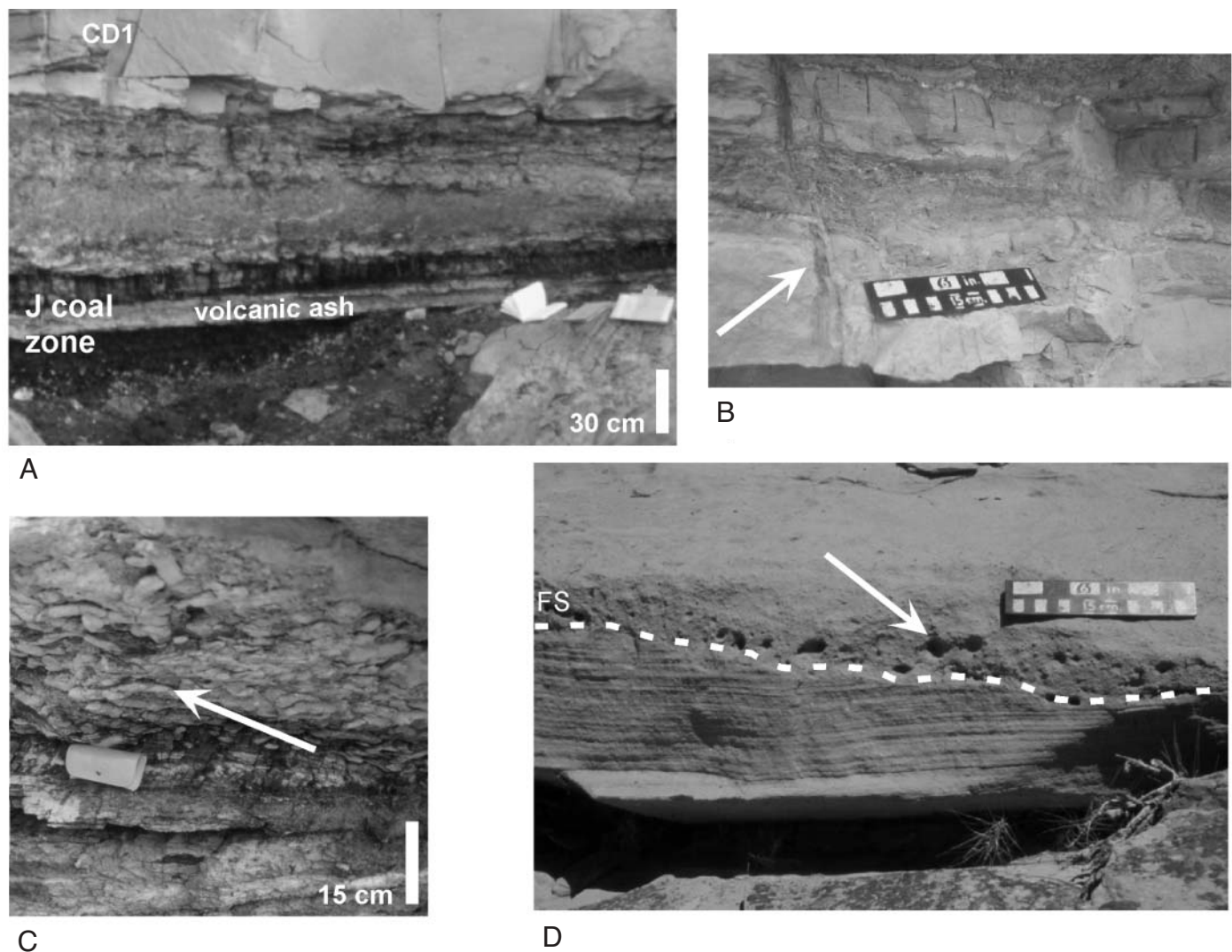


Figure 4. (A) Example of paleosols and coal zone with volcanic ash layer that underlie the channel deposits CD1 sandstone; (B) example of root-ed (arrow), very fine, ripple cross-laminated sandstone; (C) example of *Teredolites* burrows (arrow) within coalified logs; (D) transgressive lag deposits containing *Ophiomorpha* (arrow) that represents the flooding surface (dashed white line FS) that caps SC7.

The mapped location of the paleo-shoreline at only 24 km (15 mi) north (Garrison et al., 1997) and the presence of marine, wood-boring trace fossils such as *Teredolites*, which are common in the underlying flood-plain at Corbula Gulch, show that the delta plain experienced periodic marine inundation, followed by subaerial exposure. The channel deposits at Corbula Gulch are thus interpreted to be deposited on a marine-influenced lower delta plain.

The upper boundary of SC7 is a flooding surface (Garrison et al., 1997) represented locally by a transgressive-lag deposit containing *Ophiomorpha* burrows (Figure 4D). Most of this surface is absent from Corbula Gulch due to erosion.

METHODS AND DATABASE

The site at Corbula Gulch contains two cliff faces oriented approximately east-west and north-south (Figure

5). The cliff faces present horizontal and vertical exposures of about 1000 m (3300 ft) and 15 m (50 ft), respectively.

In order to reference the data in space to a unique datum, the study area was mapped in absolute coordinates using a combination of global positioning system (GPS) and a laser range-finder system (Xu, 2000). An accurate terrain model was generated (Xu, 2000).

The Ferron Sandstone is tilted a few degrees toward the northwest in the Corbula Gulch area. To represent the true depositional dip of the bedset surfaces we removed the regional dip of the Ferron outcrop. To compute this regional dip of the Ferron at the Corbula Gulch site, the J coal horizon was assumed to have been horizontal initially. The coal horizon was mapped at different outcrop locations with decimeter accuracy over a 1 km² (0.6 mi²) area around Corbula Gulch using a laser range finder, referenced to absolute GPS positions (Xu, 2000). A plane is fitted through the range-finder points

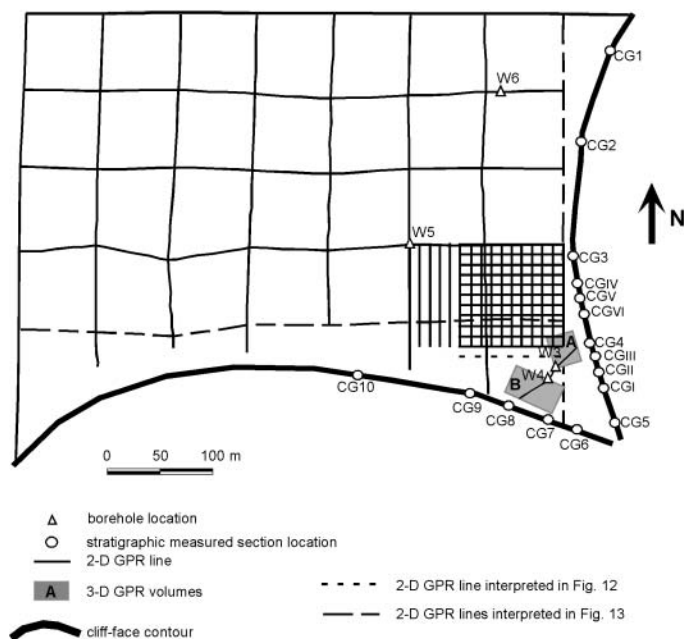


Figure 5. Map of the GPR survey site at Corbula Gulch showing the location of the 3-D GPR surveys and 2-D GPR lines on the flat mesa top related to the cliff-face outcrop positions. CG1 to CG10 are locations of measured stratigraphic sections at the cliff face. CGI to CGVI are location of short measured sections at the cliff face. W3 through W6 are locations of drill holes from which cores were extracted.

with known (x, y, z) coordinates yielding a strike of 038° and a dip of 2.5° northwest (Xu, 2000). The regional dip, computed at Corbula Gulch, is very similar in magnitude and orientation with the regional dip of the Ferron documented by previous workers (Ryer, 1981; Barton, 1994; Garrison et al., 1997).

Cliff-Face and Drill-Hole Data

The geologic data collected at Corbula Gulch include detailed facies maps both the east-west and north-south-oriented outcrops (Figures 5 and 6), ten stratigraphic sections (CG1 through CG10) evenly spaced along both outcrops (Figure 6), and four 16-m-long (55-ft), 6.3-cm (2.5 in.) cores obtained from drill holes behind the outcrops (W3 through W6). The bounding surfaces identified in the outcrop were also correlated with drill-hole cores. Paleoflow measurements from cross-strata are also recorded (Figure 6).

In order to describe inaccessible exposures we used a telescope with 60X magnification. Where possible we accessed the outcrop directly to document in detail the mudstone drapes and mudstone-intraclast conglomerate layers inside the channel deposits. The mudstone and mudstone-intraclast conglomerate layers are interpreted as the most important potential fluid-flow barriers within channel-sandstone reservoirs and were mapped in detail.

Permeability measurements were performed on core plugs extracted from the outcrop along each stratigraphic section at a sample spacing of 0.1 m (0.3 ft). A probe permeameter was used to test one end of each core plug. The permeability measurements on drill-hole cores were made at sample spacing of 0.05 m (0.16 ft) using a computer-controlled, stage-mounted, electronic probe permeameter.

Ground-Penetrating Radar Data

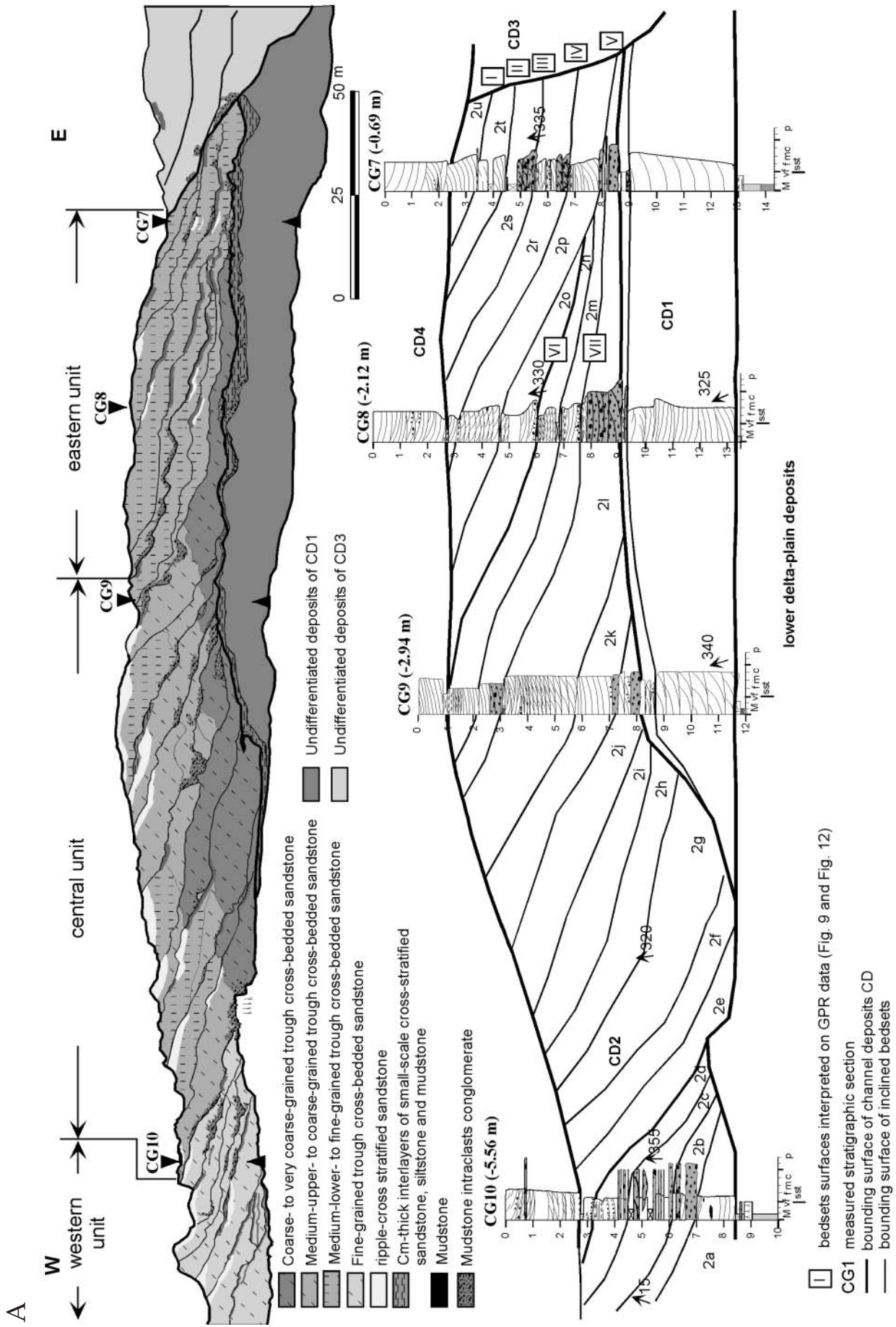
Ground-Penetrating Radar Overview

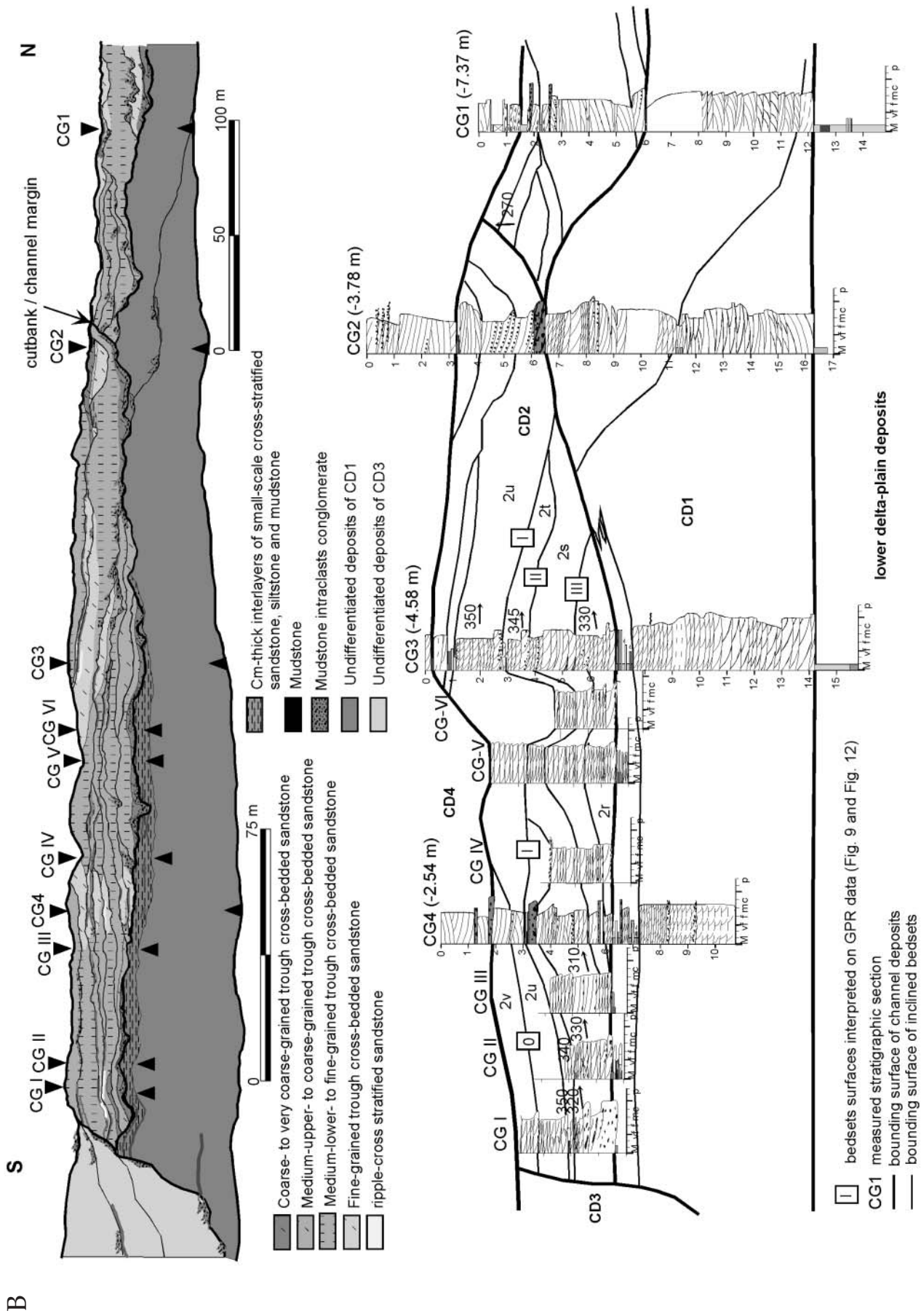
Ground-penetrating radar is a high-resolution geophysical technique that is based on recording the energy from an electromagnetic pulse that is reflected and diffracted at natural boundaries that have high contrast in electromagnetic properties (Davis and Annan, 1989). For ancient sedimentary rocks of mixed sandstone and mudstone lithology, the depth of penetration and vertical resolution can be on the order of 10-15 m (33-49 ft) and 0.25-0.5 m (0.82-1.6 ft), respectively, depending on the recording frequency and the electrical properties of the rocks (Szerbiak et al., 2001). The maximum depth of penetration depends on attenuation of the GPR signal. The attenuation decreases as the effective electrical resistivity increases and as the signal frequency decreases. The vertical resolution depends on the propagation velocity of electromagnetic waves and the signal bandwidth, which in turn depends mainly on the complex dielectric permittivities of the materials encountered and the dominant frequency in the source, respectively (Davis and Annan, 1989). There is always a trade off between maximum depths of penetration, obtained at low frequencies (e.g., 25 or 50 MHz) and the minimum dimension of features that are resolved at high frequencies (e.g., 200 MHz or more).

Flat, barren mesas, like those found at the top of the Ferron Sandstone outcrops, represent optimal environments for application of GPR technology. A shallow ground-water table will strongly attenuate the GPR signal in the saturated zone below the water table. In well-drained semi-arid environments, such as the site discussed in this paper, the water table is sufficiently deep that it is not the limiting factor for optimizing the depth of penetration.

Ground-Penetrating Radar Acquisition and Processing

The GPR survey covers three different orders of areal extent frequently used in flow-simulation studies, and consists of 2-D and 3-D GPR data sets (Figure 5). The dimension of one large grid unit in a reservoir model, equivalent to an inter-well distance, is covered by the large 2-D GPR grid in Figure 5. The dimension of





a typical voxel (volume pixel) in a reservoir flow simulator (Dreyer, 1993; Lowry and Jacobsen, 1993) is represented by the small 3-D GPR volumes in Figure 5. To link the two sets of GPR data, a third survey of 2-D GPR lines of intermediate scale was acquired.

We recorded two 3-D common-offset digital GPR data sets (50 m x 28 m [164 ft x 92 ft] and 31 m x 22 m [102 ft x 72 ft], respectively) with inter-line and inter-trace spacing of 0.5 m (1.6 ft). A survey consisting of 100 m x 100 m (328 ft x 328 ft) grid of 2-D common-offset GPR lines oriented north-south and east-west at 10 m (33 ft) spacing between lines, and 0.25 m (0.82 ft) spacing between traces on each line was also acquired (Figure 5). Finally, we recorded a 375 m x 550 m (1230 ft x 1806 ft) grid of 2-D common-offset GPR lines oriented north-south and east-west with 75 m (246 ft) spacing between lines, and 0.5 m (1.6 ft) spacing between traces on each line. A PulseEKKO IV GPR system with a transmitter voltage of 1000 V was used to collect all GPR data sets. The half-wave dipole antennas were oriented parallel to each other and perpendicular to the survey lines at an offset of 3 m (10 ft) and a central recording frequency of 100 MHz (resulting in a vertical resolution of about 0.5 m [1.6 ft]) in all surveys. Common-midpoint data were collected at 50, 100, and 200 MHz to determine optimal recording parameters and to estimate the propagation velocity. Drill-hole GPR data sets were recorded at four drill holes (Figure 5) to allow high-accuracy estimation of the vertical velocity distribution within the 3-D GPR volumes (Hammon et al., 2002).

All GPR data sets were pre-processed and the two 3-D GPR cubes and intermediate grid of 2-D lines were depth migrated before interpretation. Pre-processing included trace editing, direct wave removal (to reduce near-surface interference), time zero correction, band-pass filtering (to discriminate high-frequency events associated with subtle sedimentary features from high-amplitude energy near the median signal frequency), topographic corrections, and gain analysis (to compensate for the rapid attenuation of the signal). The pre-processing techniques used in GPR surveys are fully described by Szerbiak et al. (2001). Velocity analysis included estimation of one-dimensional vertical velocity profiles at wells and measured sections, and interpolation between these profiles to obtain a 3-D velocity model. Finally, a 3-D pre-stack Kirchhoff depth migration was applied to provide direct and accurate 3-D correlation of the geologic features and the GPR reflections. The vertical sampling of the depth migrated data is 0.1 m (0.3 ft). Due to signal attenuation in the mudstone layers in the first few meters below the surface, the 100 MHz GPR data had a maximum penetration depth of about 10 m (33 ft), so we are able to investigate with the GPR only the inclined heterolithic beds of the channel deposits.

General Ground-Penetrating Radar Interpretation

The similarities between GPR data and seismic data allow the procedures developed for interpreting 3-D seismic data (Brown, 1996) to be successfully utilized in 3-D GPR investigations (Beres et al., 1995; Hornung and Aigner, 2000; Corbeanu et al., 2001). Both 3-D GPR volumes at Corbula Gulch were examined repetitively on in-line and cross-line profiles and on horizontal slices to spatially map the inclined beds observed in outcrop. Unlike 2-D lines that may or may not be recorded parallel to the dip direction of the beds, a 3-D cube may be sliced arbitrarily according to different azimuths suggested by the sedimentologic interpretation. Also, detailed interpretation of the 2-D GPR intermediate-scale data set was possible by interactive correlation with the 3-D GPR interpretation using seismic interpretation software that permitted a direct link between different 2-D and 3-D data sets. Ground-penetrating radar interpretation is built on the principles used in seismic stratigraphic interpretation (Vail, 1987; Gawthorpe et al., 1993; Corbeanu et al., 2001; and many others). For example, a radar facies is similar to a corresponding seismic facies; both are units mapped in 3-D with distinct shape and composed of groups of reflections with specific configuration, continuity, amplitude, frequency, and interval velocity, recognizably different from adjacent radar/seismic facies (Baker and Monash, 1991; Gawthorpe et al., 1993). A radar sequence is used in this paper to describe a relatively conformable succession of GPR reflections that are discordant with surrounding reflections. The discordances match the erosional surfaces associated with different channel elements. Ground-penetrating-radar reflections can be generated at bedding planes, fracture planes, or any other boundary separating rock types with different electrical properties. Electrical properties of a rock correlate mainly to lithologic composition (sand/clay ratio, grain size, sorting, etc.) and water saturation, which is generally a measure of permeability and porosity of rocks (Knight and Nur, 1987; Annan et al., 1991; Rea and Knight, 1998). The main geologic surfaces that produce GPR reflections at Corbula Gulch are layers with high clay content as mudstone drapes and mudstone-intraclast conglomerate layers. We also made use of various GPR attributes such as instantaneous amplitude, frequency, and phase to recognizing complex interfaces of layers with small thickness (Tanner et al., 1979; Robertson and Nogami, 1984).

SEDIMENTARY FACIES

Four channel deposits (CD) were identified within the sandstone body and are referred to as channel deposits CD1 to CD4, in ascending stratigraphic order (Figures 7A and 7B). These channel deposits are com-

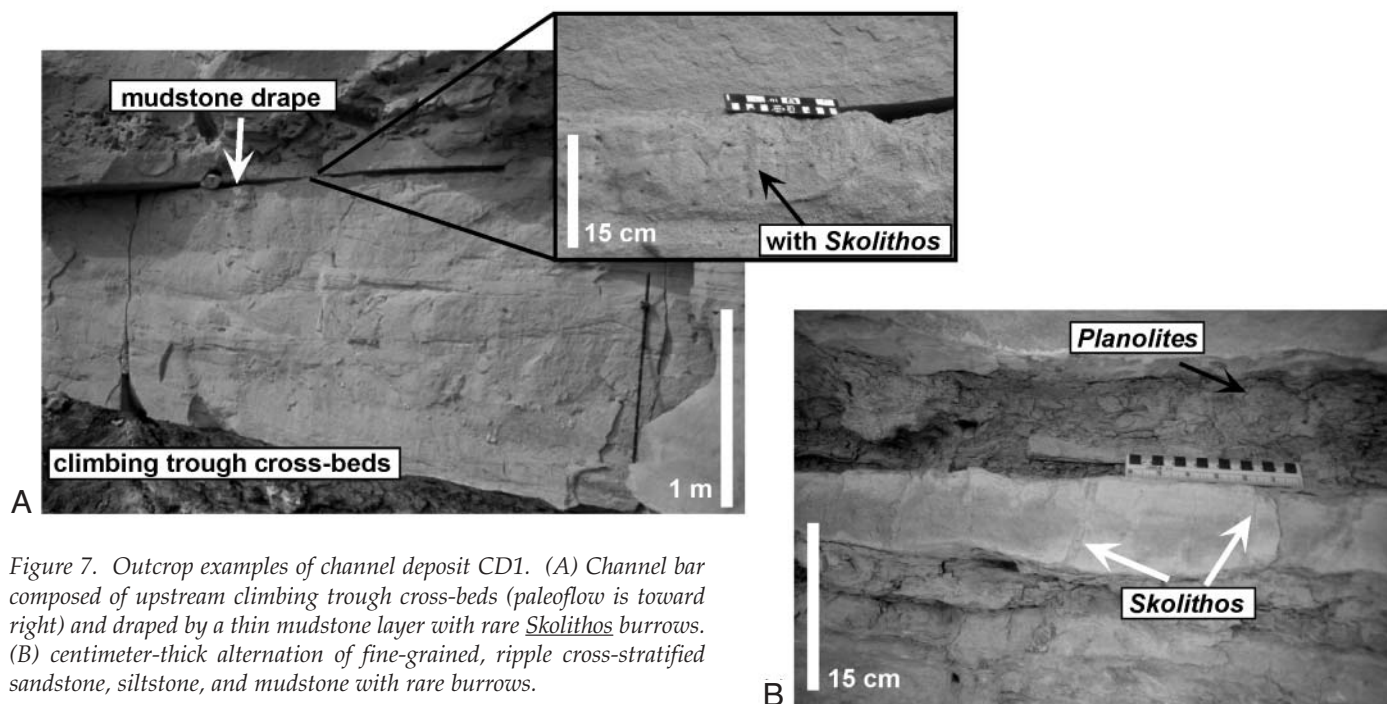


Figure 7. Outcrop examples of channel deposit CD1. (A) Channel bar composed of upstream climbing trough cross-beds (paleoflow is toward right) and draped by a thin mudstone layer with rare *Skolithos* burrows. (B) centimeter-thick alternation of fine-grained, ripple cross-stratified sandstone, siltstone, and mudstone with rare burrows.

posed of a set of more-or-less conformable, large-scale inclined bedsets and have erosional basal surfaces. Each channel deposit is characterized by complex internal features including lithofacies, bedding features, and erosional features, and distinctive external shapes. Channel deposit CD2 is characterized also by internal GPR features of specific radar facies, and GPR reflection termination at the bounding surfaces.

Channel Deposit 1

The lowermost channel deposit in the succession, CD1, varies in thickness from 0-7 m (0-23 ft) and has a basal erosion surface (Figure 6). Channel deposit CD1 is tabular to lenticular and is truncated by basal erosional surface of CD4 and CD3 (Figure 6). The paleoflow direction measured from trough cross-beds and basal scours is toward the north-northwest (azimuth 310° to 350°).

Channel deposit 1 consists mainly of trough cross-bedded sandstone and planar cross-bedded sandstone that in places form 1-2 m (3-6 ft) thick, coarsening- or fining-upward co-sets. Trough cross-beds in CD1 typically climb in an upstream direction (Figure 7A) and the co-sets are draped locally by centimeter-thick mudstone layers containing *Skolithos* burrows (Figure 7A). These mudstone drapes extend for 15-20 m (49-66 ft) in the paleoflow direction (Figure 7B). The upper part of CD1 is a 0.25-0.5-m (0.8-1.6-ft) thick alternation of thin, fine-grained, ripple cross-stratified sandstone and/or siltstone, and mudstone. In the fine sandy and silty layers are rare *Skolithos*, *Planolites*, and *Thalassinoides* burrows.

The mudstone-draped co-sets in the lower part of CD1 are interpreted as abandoned fluvial bars (Bridge,

1985). The presence of some brackish-water burrows suggests marine influence during channel abandonment. The upward climbing of the cross-bed co-sets in the upstream portion of the barform (Figure 7A) implies that sedimentation rates were high and that bar accretion occurred both in an up-current and down-current direction (Bridge, 1985; Miall and Turner-Peterson, 1989). The uniform nature of trough cross-bedded sandstone of CD1 and the low variance of the paleocurrent data (Figure 6) suggest that CD1 was deposited in a low sinuosity distributary channel. The fine-grained deposits in the upper part represent the abandonment stage of the distributary channel (Figure 7B).

Channel Deposit 2

Sedimentologic Description

Channel deposit 2 consists of a series of low-angle, inclined bedsets dipping apparently toward the east (Figure 6A) that are similar to the inclined heterolithic stratification (IHS) and inclined stratification (IS) of Thomas et al. (1987). Channel deposit 2 has a generally erosive base with moderate local relief, and cuts into the underlying deposits of CD1. Channel deposit 2 cuts directly into underlying muddy delta-plain deposits in places where it removes CD1 (Figure 6A). Channel deposit 2 has a tabular shape and a mean thickness of about 7 m (23 ft), and is truncated toward the east and south by CD3 and on top by CD4 (Figure 6). Toward the north, CD2 cuts into another unit composed of inclined bedsets dipping south (Figure 6B).

Each inclined bedset cuts erosionally into the under-

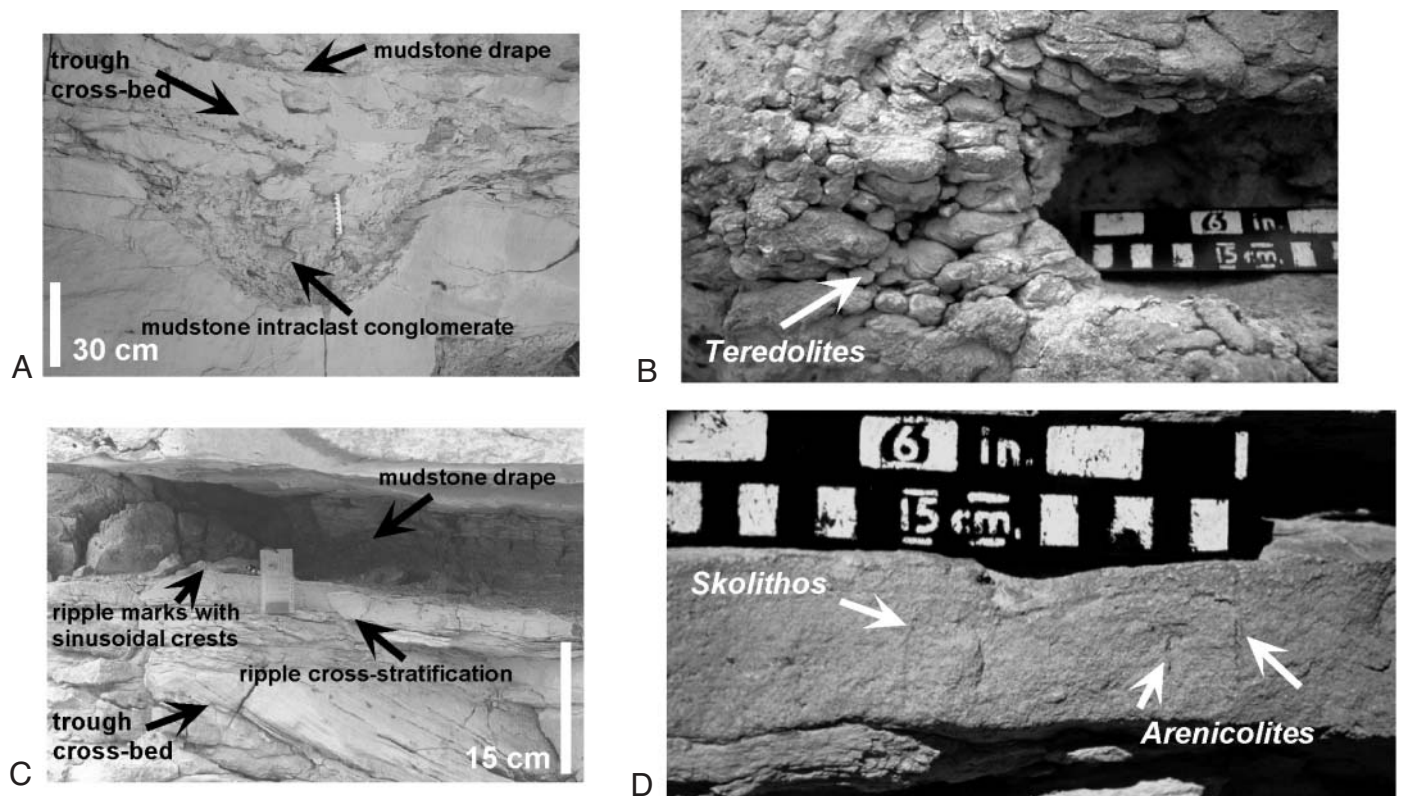


Figure 8. Facies and trace fossils characteristic of channel deposit CD2. (A) Mudstone intraclast conglomerate along the erosional basal bounding surfaces of an inclined bed; (B) *Teredolites* burrows common within the fossilized log fragments within the basal conglomerate; (C) trough cross-bedded sandstone, ripple cross-laminated, fine-grained sandstone/siltstone and mudstone facies succession typical of inclined beds within CD2; and (D) *Skolithos* and *Arenicolites* burrows in the upper parts of the inclined bedsets.

lying inclined bedset and forms an accreting unit. Commonly, the basal bounding surface of the inclined beds contains mudstone intraclast conglomerates along scours (Figure 8A). The mudstone intraclast conglomerate beds can locally reach more than 1 m (3 ft) thickness within deep scours and can contain mudstone clasts and woody debris up to 0.5 m (1.6 ft) long. The coalified woody debris commonly contains extensive *Teredolites* burrows (Figure 8B). Laterally, mudstone intraclast conglomerate beds have small extent up to 4-5 m (13-16 ft) in outcrop. Inclined bedsets fine upward and generally contain trough cross-bedded to ripple cross-laminated sandstone and decimeter-thick alternation of siltstone/mudstone beds and mudstone drapes (Figure 8C). The siltstone/mudstone beds and mudstone drapes are 0.1-0.2 m (0.3-0.7 ft) thick, but extend downdip, parallel to the inclined surfaces of the beds, up to 7-8 m (23-26 ft) and occasionally more than 10 m (33 ft) in outcrop. Rare *Skolithos*, *Arenicolites*, (Figure 8D) *Planolites*, and *Thalassinoides* burrows occur in the upper, fine-grained parts of these inclined bedsets.

In the west-east outcrop we identified three different units of inclined bedsets characterized by specific grain-size, thickness of beds, and facies (Figure 6A).

The western-most unit of inclined bedsets (Figure 6A) is about 6 m (20 ft) thick and consists of bedsets dip-

ping at 5° east. The thickness of each inclined bedset is between 1 and 2 m (3 and 6 ft). Internally, these inclined beds consist mostly of low-angle to parallel-laminated and rarely trough cross-bedded sandstone, and ripple cross-laminated, fine-grained sandstone. In the most western part of this unit, the inclined bedsets are composed entirely of fine-grained, ripple cross-laminated sandstone. Each inclined bedset has an erosional basal bounding surface with mudstone intraclast conglomerate along scours and is capped by a decimeter-thick mudstone layer. In the eastern part of the unit, the mudstone intraclast conglomerate is more common along the erosional scours than in the western most part. Overall, within the bedset unit, there is a decrease in mudstone content laterally, in the direction of bed dip. Paleoflow direction measured from trough cross-beds is north (azimuth of 355° to 015°).

The central unit of inclined bedsets (Figure 6A) is about 7 m (56 ft) thick and consists of bedsets dipping more steeply at 8-10° eastward. The thickness of each inclined bedset is between 1.5 m and 3 m (4.9 ft and 10 ft), and the mean thickness of the trough cross-bed sets is about 0.14 m (0.46 ft) with an overall, upward thinning of the cross-bed sets (CG9 in Figure 6A). The inclined bedsets consist of very coarse- to medium-grained, trough cross-bedded sandstone to fine-grained, ripple

cross-laminated sandstone. Locally, decimeter-thick mudstone drapes separate the inclined beds. The lower part of the unit of bedsets is mainly composed of coarse- to very coarse grained trough cross-bedded sandstone with mudstone intraclast conglomerates scattered along foresets. Locally, the upper part of the central unit of bedsets consists of fine-grained, ripple cross-laminated sandstone. Overall, within the unit of bedsets, there is a decrease in grain size upward and in the direction of bedset dip. The paleoflow measured from trough cross-beds is toward the northwest (azimuth 320°).

The eastern-most unit of inclined bedsets (between CG8 and CG7 in Figure 6A) is about 6 m (20 ft) thick and consists of bedsets dipping less steeply than the central bedset, at 5° toward the east. Thickness of inclined bedsets ranges from 1-1.5 m (3-4.9 ft), and the mean thickness of the trough cross-bed sets is 0.13 m (0.43 ft). Each inclined bedset consists of medium-grained, trough cross-bedded sandstone to very fine grained ripple, cross-laminated sandstone to mudstone. Within each inclined bedset there is a distinct upward-fining trend perpendicular to the inclined bounding surface of the bedset. The basal bounding surface of each bedset is erosional and is locally overlain by mudstone intraclast conglomerate. Mudstone drapes are parallel with the inclined bounding surface of the bedsets and is locally discontinuous due to erosion. Overall there is more mudstone in the central and eastern part of this unit of bedsets. Paleoflow measured from trough cross-beds is northwest (azimuth 330° to 335°).

Part of the eastern-most unit of inclined bedsets crops out in the north-south cliff face and the inclined beds are nearly horizontal, slightly convex upward surfaces. Each inclined bed consists of medium-grained, trough cross-bedded sandstone and in the southern part of the outcrop of coarse- to medium-grained, trough cross-bedded sandstone to fine-grained, ripple cross-laminated sandstone to mudstone. In places, especially toward the central and northern part of the outcrop, the inclined beds consist only of medium-grained to fine-grained sandstone. The mudstone drapes are discontinuous and present mostly in the southern and northern part of the outcrop. Paleoflow measured from trough cross-beds is generally northwest and varies vertically from azimuth 310° , 320° , and 330° in the lower part of the bedset to 345° and 350° in the upper part.

Ground-Penetrating Radar Interpretation

The GPR interpretation is focused on CD2. The bounding surface between CD2 and CD4 on the GPR record is not a continuous reflection, but a surface that envelops the truncations and top lap terminations of the oblique reflections below (Figures 9 and 10). The bounding surface between CD2 and underlying CD1 is a composite reflection produced by the downlapping termina-

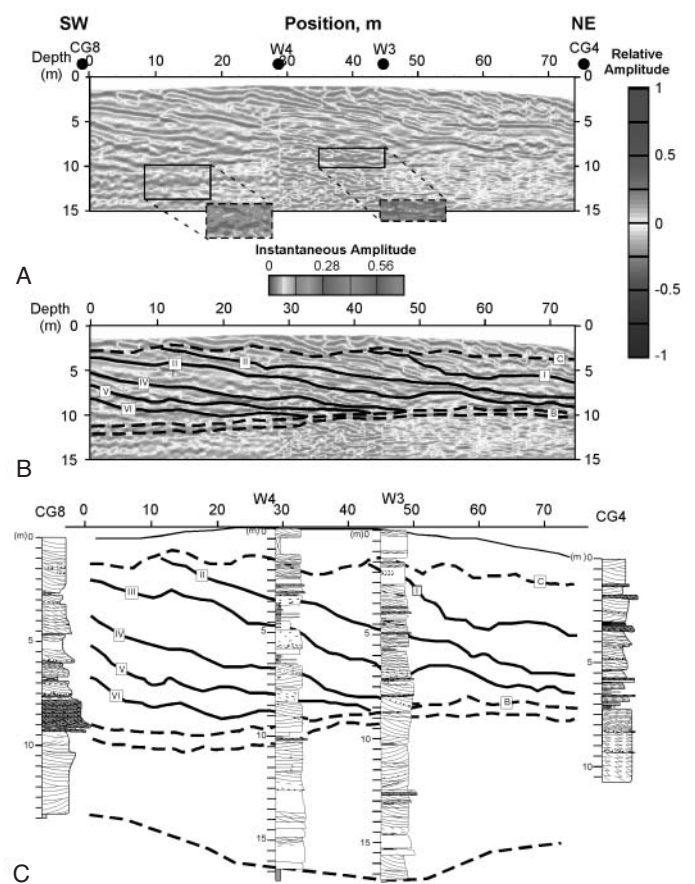


Figure 9. Ground-penetrating radar traverse line from CG8 to CG4 through both 3-D GPR volumes (Figure 5). The middle portion, between W4 and W3, is a 2-D GPR line that links the interpretation from the two data cubes. (A) Uninterpreted and (B) interpreted GPR reflections as inclined surfaces (0 to V) within CD2. Surfaces B and C are respectively the basal and top bounding surfaces of CD2. Notice the inclined, continuous, high-amplitude reflection that characterizes the main radar facies within CD2 (also in Table 1). Rectangular insets show examples of composite reflections resulting from constructive interference from thin layers. These composite reflections are resolved in the GPR instantaneous amplitude display. (C) Cross section showing the correlation between the 3-D GPR interpretation and the outcrop and drill-hole lithologic columns. CG8 and CG4 are projected from 6 m (20 ft) and 10 m (33 ft), respectively, onto the GPR profile.

tions of the inclined reflections with long tangential toes. Mudstone drapes on the top surface of inclined bedsets produce good contrast in electrical properties and give rise to readily identifiable GPR reflections. The mudstone intraclast conglomerate beds at the bases of the inclined bedsets can also produce GPR reflections. The surfaces separating cross-stratification sets can produce GPR reflections if there is significant variation in grain size, but the electrical contrast is very small, and the reflections have low amplitudes and are discontinuous (Gawthorpe et al., 1993; Bridge et al., 1995; Corbeau et al., 2001). In many cases these boundaries do not have the same orientation and dip as the inclined bedsets, and interfere constructively or destructively with the

stronger reflections given by the inclined bedsets producing composite reflections.

Ground-penetrating radar interpretation of the three-dimensional data sets: Channel deposit 2 represents a radar sequence composed of high-amplitude, continuous, oblique GPR reflections dipping at an angle of 6-8° northeast (Figures 9A and 9B). Each inclined bedset was identified on outcrop (Figure 9C) and then interpreted throughout both 3-D GPR volumes. Where the inclined beds are thinner than the vertical resolution of 0.5 m (1.6 ft), composite reflections can cause interference of high positive or negative amplitudes due to tuning effects. These composite reflections were interpreted by analyzing other GPR attributes like instantaneous amplitude (Figure 9B).

A horizontal slice through both volumes at a depth of about 5 m (16 ft) shows the general structure of dipping beds toward the northeast, consistent with the sedimentologic interpretation (Figure 11). There is a slight change in the strike of the inclined reflections from Grid B to Grid A, from azimuth 340° to azimuth 320°, respectively. The radar facies interpreted to compose the radar sequence CD2 in the 3-D GPR volumes are presented and described in Table 1.

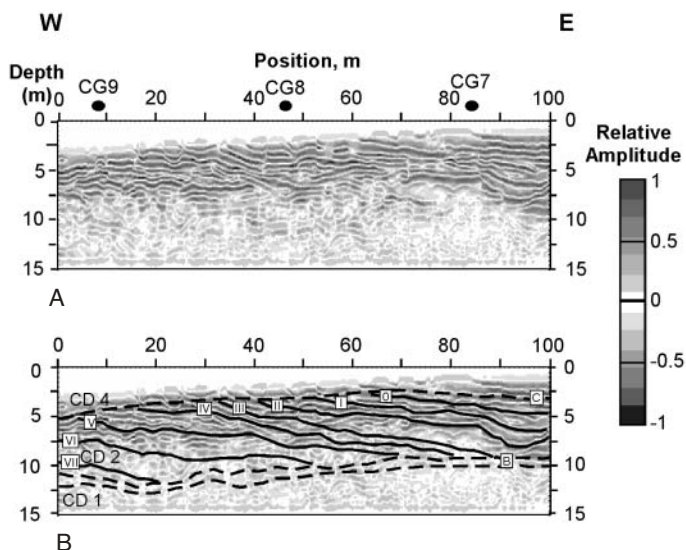


Figure 10. (A) Uninterpreted and (B) interpreted GPR line from the intermediate (100 m x 100 m [328 ft x 328 ft]) 2-D GPR grid (Figure 5). The interpretation shows a series of inclined surfaces dipping east and correlating with the 3-D GPR cubes (Figure 9) and outcrop (Figure 6). Recognized GPR facies are described in Table 1. CG7 to CG9 are the projections of the measured sections at the cliff face onto the GPR lines. Surfaces B, C, and 0 to VII are the same as in Figures 6 and 9.

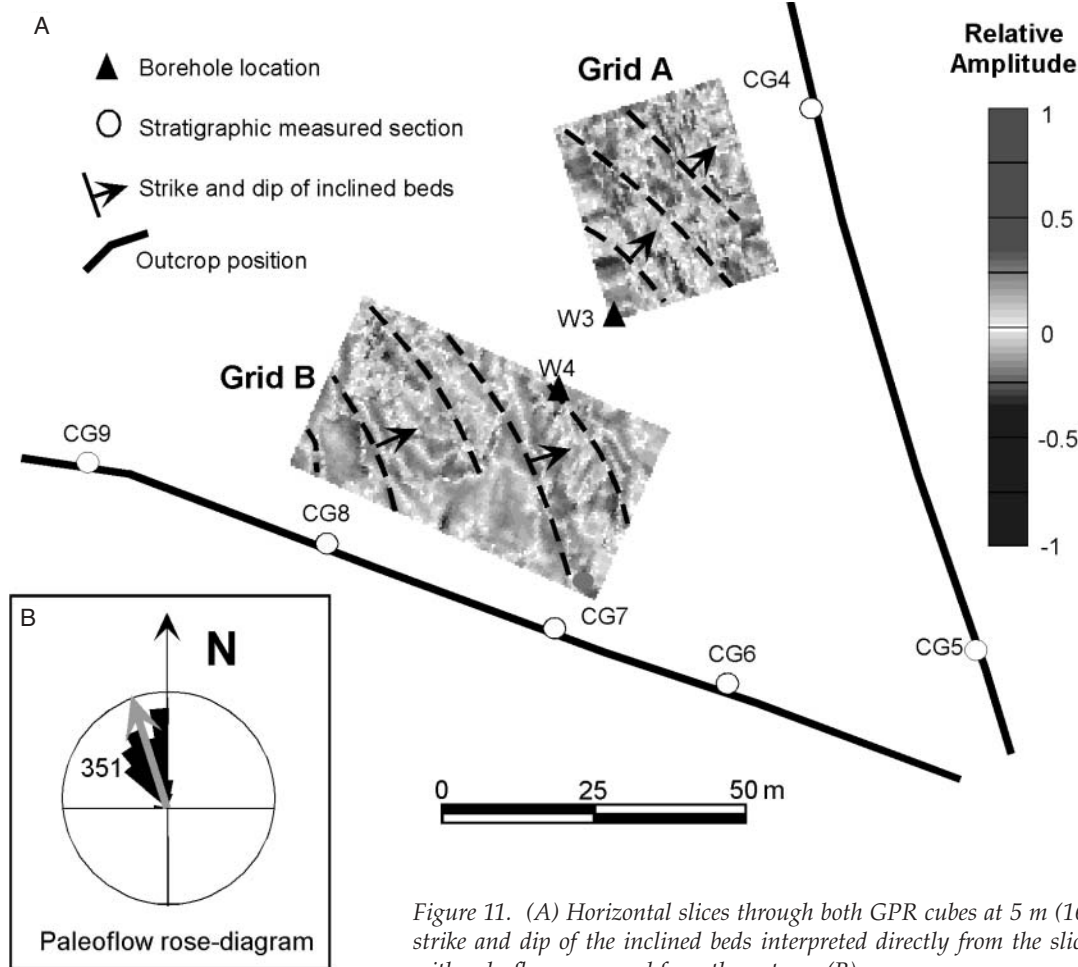
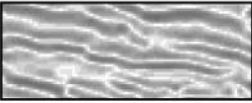
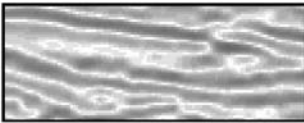
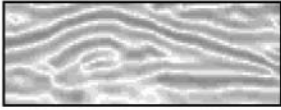
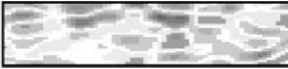


Figure 11. (A) Horizontal slices through both GPR cubes at 5 m (16 ft) depth. The strike and dip of the inclined beds interpreted directly from the slices is consistent with paleoflow measured from the outcrop (B).

Table 1. Radar vs. sedimentologic facies of point-bar deposits.

GPR Reflection Configuration	Radar Pattern	Sedimentologic description
High amplitude, oblique, parallel reflections		Lateral accreting surfaces of point bar Inclined Heterolithic Stratification (view perpendicular on depositional dip)
High amplitude, oblique, continuous, concave upward reflections		Lateral accreting surfaces of point bar Inclined Heterolithic Stratification (view perpendicular to depositional dip)
High and low amplitude, mounded reflections		Lenticular sandstone developed on the downstream accreting part of the point bar (view parallel to depositional dip)
High and low amplitude, hummocky reflections	 	Accretionary topography on the point bar surfaces Mudstone intraclast conglomerate bodies accumulated at the base of scours
Low amplitude, chaotic reflections		Massive and/or cross-bedded sandstones without significant variation in grain size

Geostatistical analysis of three-dimensional ground-penetrating radar amplitudes: To quantify the lateral extent of mudstone and conglomerate layers inside CD2, assumed to mimic the continuity of the corresponding GPR reflections, experimental variograms are computed from the GPR relative amplitude data. Variogram modeling has been successfully used by Rea and Knight (1998) and Corbeanu et al. (2001) to characterize heterogeneities of the subsurface in 2-D and 3-D, computing the correlation lengths of radar reflections along maximum and minimum correlation directions. The assumption is that there exists a link between the lithology of layers and their electrical properties and thus a relationship between lithology and the correlation structure of GPR reflections. This spatial relationship can be expressed through standard variograms, a measure of the spatial autocorrelation of a regionalized variable (Rea and Knight, 1998; Corbeanu et al., 2001). The experimental variograms are computed from GPR relative amplitudes within the 3-D GPR facies of inclined reflections of CD2, using the equation:

$$\gamma_{(h)} = (1/2N(h)) \sum (x_i - y_i)^2 \quad (1)$$

where γ is the computed variance of GPR amplitudes, h is the separation distance between two data points (the lag), $N(h)$ is the number of pairs of data points separated by h , x_i is the data value at one of the points of the

i -th pair, and y_i is the corresponding data value at the second point (Deutsch and Journel, 1998).

The maximum correlation direction of the 3-D GPR amplitudes was inferred from the dip and strike of the inclined beds measured in outcrop, which average 8° and 340° , respectively. The minimum correlation direction is perpendicular to the maximum correlation direction. The experimental variogram along the maximum correlation direction is modeled with a simple exponential structure with the parameters: sill = 1.13, nugget = 0.2, and range = 10 m (33 ft) (Figure 12A). Ground-penetrating radar reflections are a direct response of the existence of a contrast between the mud drapes (or mudstone intraclast conglomerate beds) and the surrounding sandstone, and so the correlation of the GPR amplitude correspond, generally, to the continuity of the mudstone or mudstone intraclast conglomerate layers. The range of 10 m (33 ft), derived from modeling the variogram of GPR amplitudes, is comparable with the lengths of the mudstone drapes and mudstone intraclast conglomerate layers measured in outcrop in the dip direction. The experimental variogram along the minimum correlation direction is modeled with a nested structure composed of an exponential model with sill = 0.95, nugget = 0.0, and range = 5.3 m (17.4 ft) combined with a gaussian model with sill = 0.15, nugget = 0.0, and range = 18 m (59 ft) (Figure 12B).

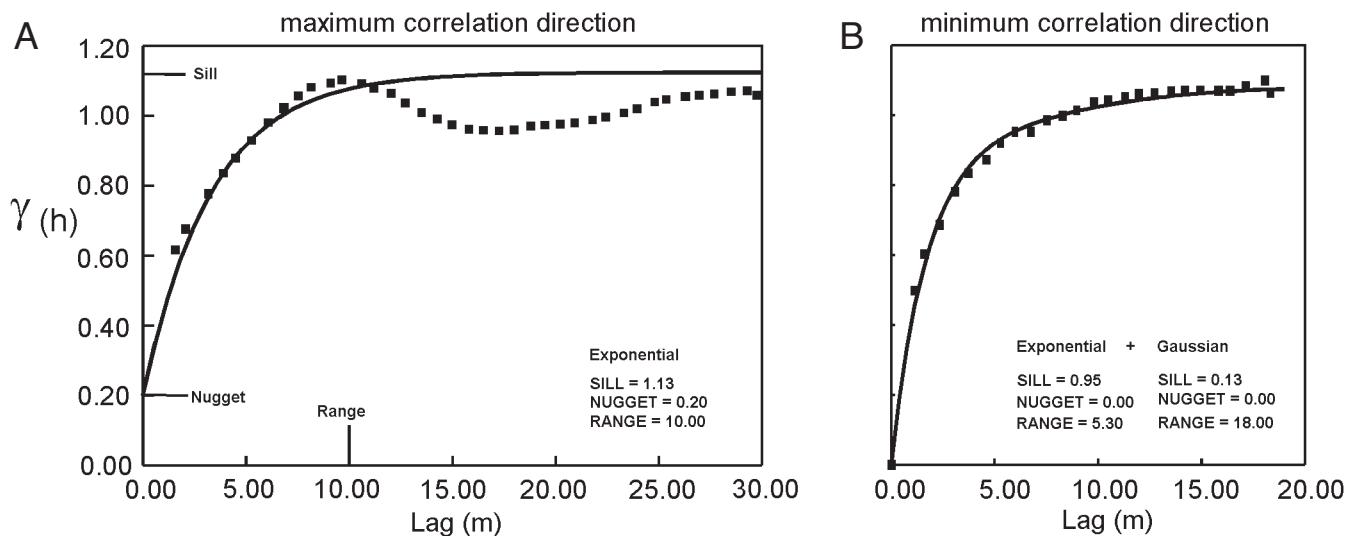


Figure 12. Experimental variograms (squares) and fitted models (continuous line) derived from the GPR amplitudes and shown along (A) maximum and (B) minimum correlation directions within CD2; the results of the variogram analysis are also presented. The nugget is the nonzero y -intercept of the experimental variogram. The sill is a constant at which the variance no longer increase and flattens. The range is the maximum distance at which the data are no longer correlated and the sill is obtained. For definitions of symbol used in the figures see equation 1 in the text.

Ground-penetrating radar interpretation of the two-dimension intermediate scale data set: The main radar sequence interpreted on the intermediate scale GPR grid corresponds also to CD2 in outcrop. The radar facies consist mainly of inclined, parallel reflections and inclined, concave upward reflections in the direction parallel to the dip of inclined beds (Figure 10). Other radar facies containing hummocky, distorted, chaotic, and less common, mounded reflection configurations were identified on the direction parallel to the paleoflow (Table 1). Each radar facies characterizes different parts of the inclined beds. The hummocky, distorted, and chaotic radar facies are characteristic of the basal down-lapping end of the inclined beds. The geometry of the inclined surfaces (Figure 10) show beds dipping between 3° and 7° east, perpendicular to the direction of the flow.

Ground-penetrating radar interpretation of the two-dimensional large scale data set: Only large scale features (GPR sequences) were interpreted in the largest 2-D GPR grid (Figure 5). This large grid was not migrated in depth like the previous GPR data sets due to lack of velocity information and well ties in the northwestern part of the survey (Figure 5). A simple time-to-depth conversion was applied using an average velocity of 0.1 m/ns.

Four different radar sequences were identified in the largest GPR grid. The radar sequence, corresponding to CD2 in outcrop, is composed mainly of inclined, parallel to concave upward reflections identified in the eastern and southern part of the grid (Figure 13). To the north, the CD2 radar sequence pinches out against a radar sequence composed of inclined, parallel reflections

apparently dipping south. The radar sequence of CD1 is composed mainly of hummocky reflections (Figure 14A). To the west, the CD2 radar sequence is truncated also by a radar sequence containing exclusively hummocky reflections, probably representing the infilling of a younger channel (Figure 13B). Only the nearest 2-D GPR lines from the outcrops were interpreted on the large scale GPR grid, because the rest of the grid was not suitable for detailed interpretation due to coarse sampling and lack of geologic control.

Integrated Sedimentologic and Ground-Penetrating Radar Interpretation

Correlating outcrop, drill-hole, and GPR data allows the relationship between vertical facies successions of the inclined beds in CD2 and their lateral geometry to be established. Two bounding surfaces from the central inclined bedset (surfaces VI and VII in Figures 6 and 14) and six bounding surfaces from the eastern-most bedset (surface 0 to V in Figures 6 and 14) were interpreted in outcrop, drill-hole, and GPR data.

The interpreted inclined surfaces migrate laterally from west to east, and also upstream (Figures 14 and 15). The strike of the inclined beds is essentially parallel with the paleoflow and rotates from a northwest-southeast direction within the central bedset (inclined surfaces VI and VII) to a north-south direction within the eastern-most bedset (inclined surfaces 0 to V). The inclined beds extend more than 250 m (820 ft) in the direction of flow based on information from the 2-D GPR large grid and north-south outcrop. This suggests that CD2 is located near the outer bank of the channel (Figures 6B and 13A).

The inclined beds of CD2 were most likely deposit-

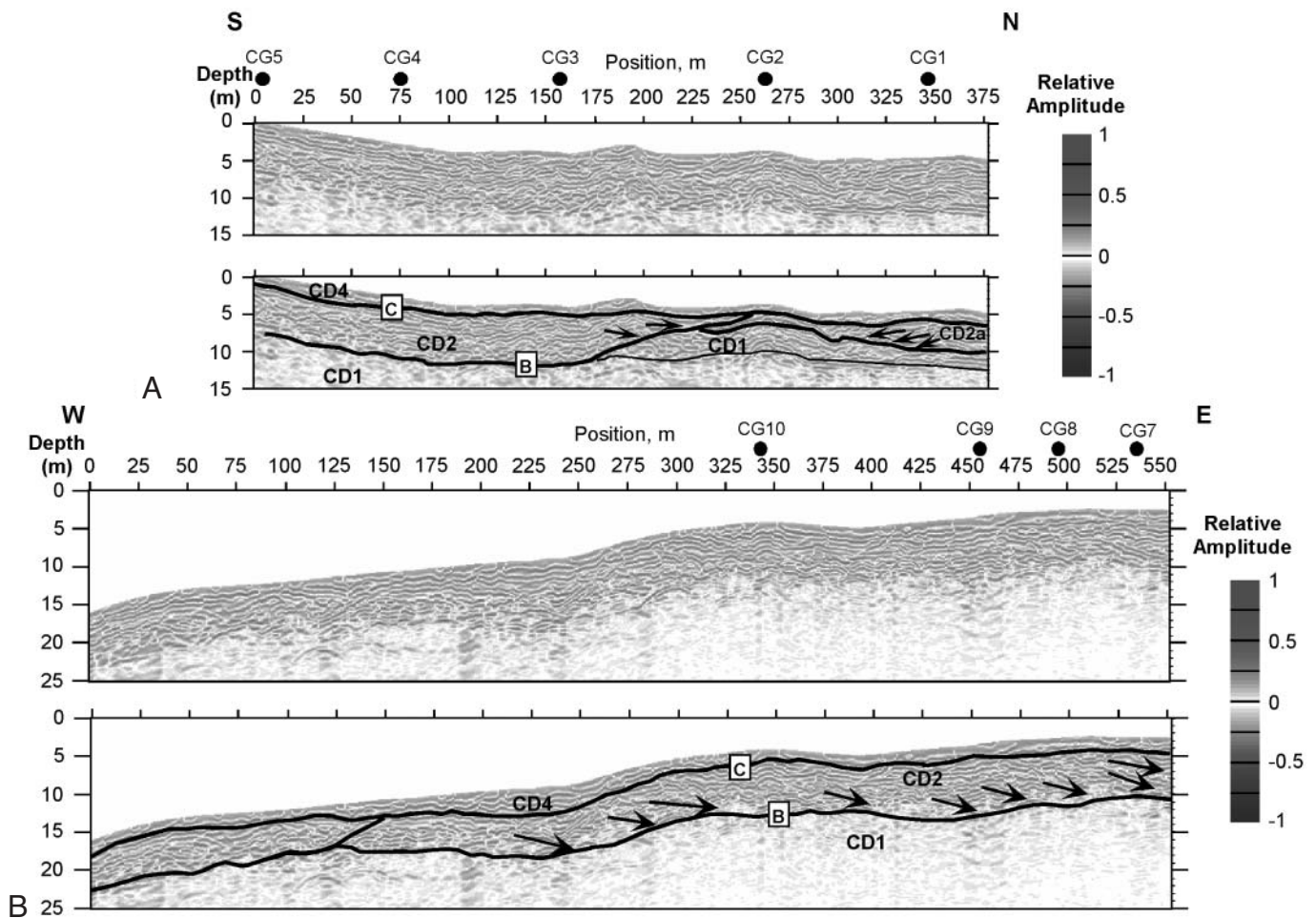


Figure 13. Two-dimensional GPR lines from the largest GPR grid parallel with the (A) south-north and (B) east-west cliff face (Figure 5). The uninterpreted and interpreted versions are displayed for correlation. CD2 deposits pinch out north against the channel cut-bank (see also Figure 6B). The westward truncation of CD2 is interpreted only from GPR data. Black arrows show the inclined beds within CD2. CG1 to CG10 are the projections of the measured sections at the cliff face onto the GPR lines.

ed by lateral and upstream accretion of a point bar within a highly sinuous distributary channel with paleoflow essentially toward the north-northwest. However, upstream migration of point bars is mostly described in tidal creeks (Thomas et al., 1987), although examples from braided rivers have also been described (Bristow, 1993). The paleocurrent directions measured in CD2 are essentially unidirectional, unlike the tidal channels that typically show bimodal paleoflow directions (Thomas et al., 1987). The marine incursions observed in CD2 are thus interpreted as seasonal, representing times of river flooding, rather than tidal. The muds drape bar-scale features rather than occurring at the scale of individual cross-strata such as the double mud drapes and sigmoidal cross-stratification diagnostic of tidal stratification (e.g. Nio and Yang, 1991). No tidal bundles, tidal rhythmites, nor double mud laminae were observed. Extensive bioturbation by *Teredolites* on large logs deposited on the basal, erosional scours of the inclined beds and within the underlying delta plain suggests marine influence (Bromley et al., 1984). The location of

the coastline 24 km (15 mi) from Corbula Gulch made possible a deposition on the lower delta plain affected by repetitive incursion of marine waters, probably related to times of seasonally low discharge. Bioturbation like *Planolites*, *Thalassinoides*, *Skolithos*, and *Arenicolites* in the siltstone/mudstone layers draping the inclined beds are also indicative of brackish water influence suggesting mixing of river and marine waters (Pemberton et al., 1992).

Paleogeometry of the Point-Bar Deposits

The most important parameters for estimating the dimensions of a meandering paleochannel are the maximum horizontal width of one inclined bed measured in direction perpendicular to the flow and the vertical depth from the toe to the top of the inclined beds (Ethridge and Schumm, 1978). These widths and depths are the expression of the bankfull channel width and the maximum bankfull channel depth, respectively (Ethridge and Schumm, 1978). The horizontal width (W)

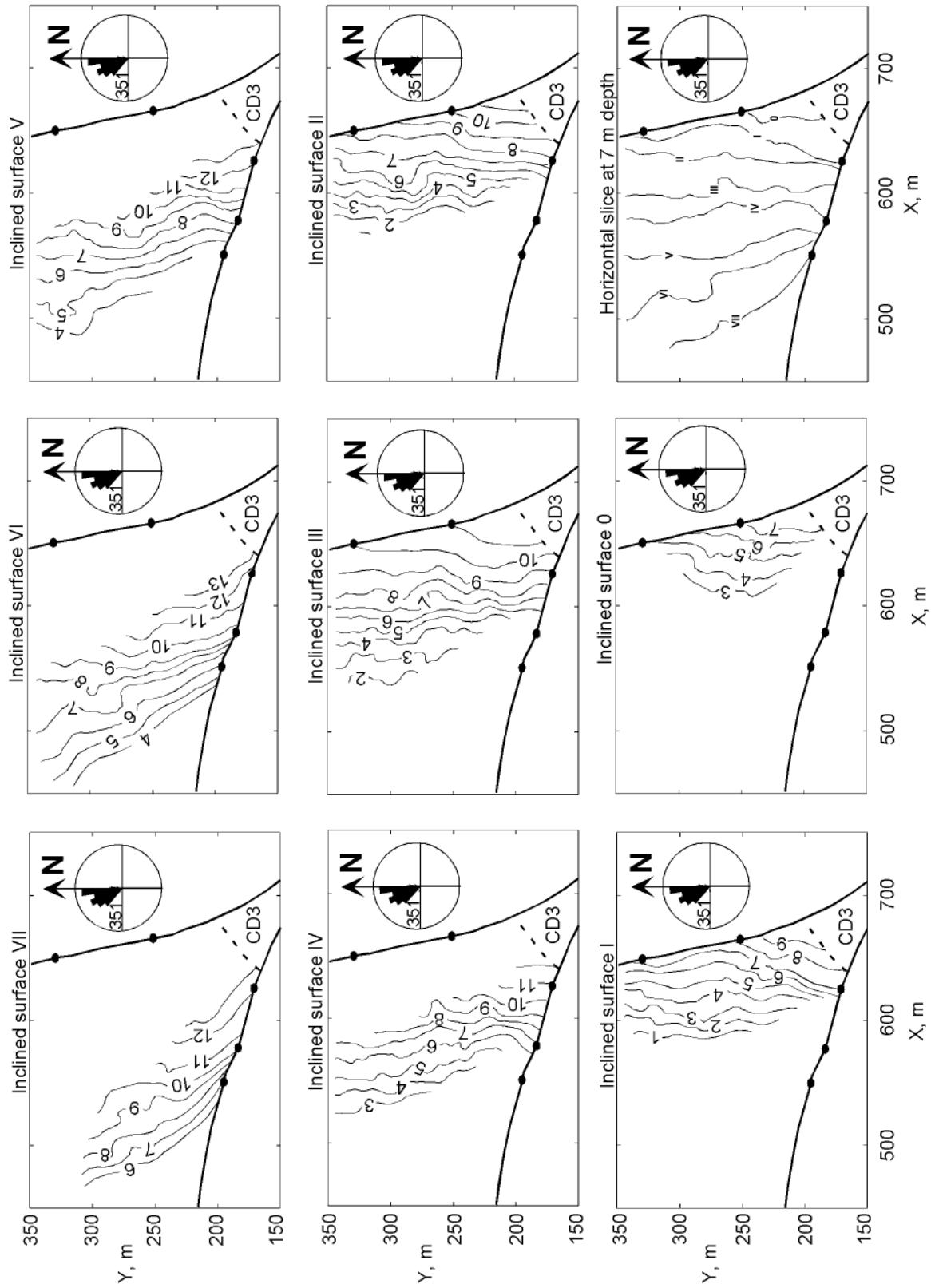


Figure 14. Depth (m) contour maps of each inclined bed interpreted from the GPR data. Surfaces 0 to VII are the same as in Figures 6, 9, and 12. The regional dip of the Ferron Sandstone outcrop (38° strike and 2.5° north-west dip) was removed to accurately represent the true depositional dip of the point-bar surfaces. The strike of the inclined beds is consistent with the paleo-flow as indicated by paleocurrent measurements in the outcrop. The dashed line represents the interpreted CD3 channel-margin. The map in the lower-right corner represents a horizontal slice through the interpreted inclined beds at 7 m (23 ft) depth. The inclined beds are generally parallel to slightly divergent toward north.

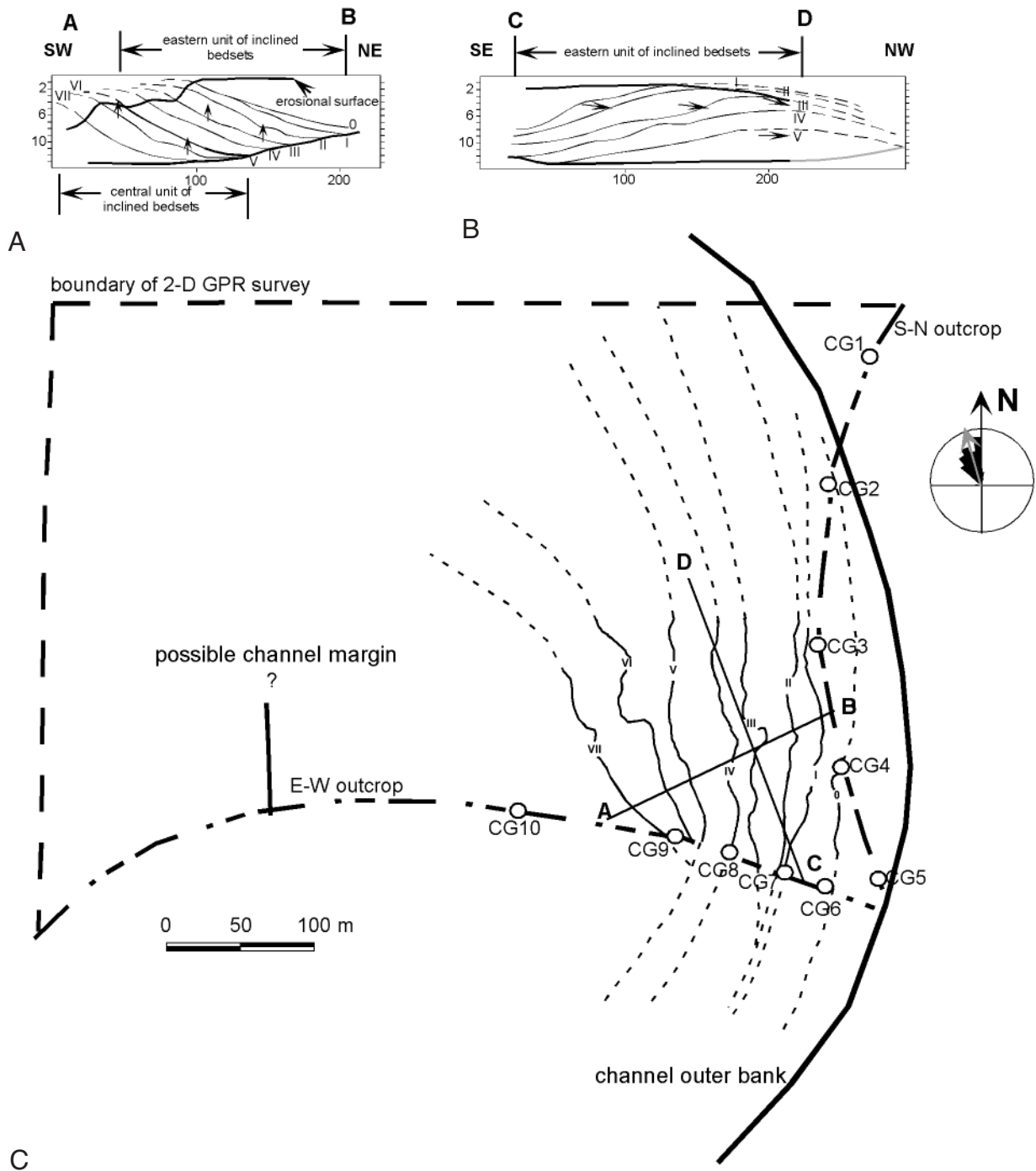


Figure 15. Vertical cross sections (A) perpendicular and (B) parallel to the flow through the interpreted point bar CD2 at Corbula Gulch. Grey lines are estimated inclined surfaces before erosion; (C) reconstruction of channel margin and inclined surfaces (VII to 0) in horizontal section at 7-m (23-ft) depth. Continuous lines are interpretation from the GPR data, dashed lines are inferred based on the local trend of each mapped inclined surface. A-B and C-D show the location of the cross sections in (A) and (B) panels.

of one inclined bed is up to 150 m (492 ft) within the central inclined bedset unit and up to 100 m (330 ft) within the eastern inclined bedset unit (Figures 6A and 14). The vertical depth (D) of an inclined bedset varies from 6 m (20 ft) within the central inclined bedset to 8 m (26 ft) within the eastern inclined bedset (Figures 6A and 14). Applying formulas used by Ethridge and Schumm (1978) to estimate the bankfull width ($W \cdot 1.5$) and mean

bankfull depth ($D \cdot 0.585 / 0.9$), resulted in a value of 225-150 m (738-492 ft) for the bankfull width of the channel and a value of 3.9-5.2 m (12.8-17.1 ft) for the mean bankfull depth. However, these values should be considered as minimum estimates because the upper part of the point bar may be completely removed by erosion associated with CD4.

The central inclined bedset shows the typical fining-

upward and thinning-upward succession of a fluvial point bar as described by Allen (1970). However, it has been demonstrated that this fining- and thinning-upward succession does not cover all possible vertical successions in meandering channels, and is characteristic only of certain models of channel migration (Bluck, 1971; Bridge and Jarvis, 1976; Jackson, 1976, 1978). Jackson (1976, 1978) showed that necessary conditions of velocity magnitude, intensity of spiral motion, and depth of channel required to produce the "standard" point bar depositional model could be reached only in the downstream parts of point bars and at moderate curved bends. Other positions along the bend can produce very different facies successions. Thus, the central bedset unit is more likely to be deposited in the downstream half of the bend, while the eastern-most bedset unit may represent deposition in a more upstream position. The eastern-most unit of inclined bedsets was deposited in a more marine-influenced environment, characterized by thinner inclined beds and more extensive mud drapes covering parts of the dip-length of the bed surfaces. The distinct fining-upward succession within each inclined bed (e.g. CG7 and CG8, Figure 6A) is interpreted to be indicative of repetitive floods characterized by flashy discharge with rapid dumping of the sediments (presence of well-developed mudstone intraclast conglomerate at the base of each inclined bed and the normal grading inside each inclined bed). Each inclined bed is interpreted as the deposit of one flood event (Thomas et al., 1987). The mudstone drape represents fines settling out from suspension at much-reduced velocity, probably a consequence of marine influence. At times of lower discharge, the salt wedge at the downstream end of the distributary channel can migrate tens of kilometers upstream (e.g. Nelson, 1970).

The different units of inclined bedsets described in outcrop and identified in GPR appear to represent successive, major phases in the growth history of a single point bar affected by seasonal variations in discharge with marine influence (Figure 15).

Channel Deposit 3

Channel deposit 3 cuts deeply into the underlying CD1 and CD2 deposits and is confined to the southwest edge of the outcrop. Channel deposit 3 has a highly erosive base with a maximum relief of about 10 m (33 ft) over a lateral distance of 50 m (164 ft) (Figure 6) and contains thick basal mudstone intraclast conglomerates along the scours. Internally, CD3 consists mostly of bedsets of 3-4.5 m (10-15 ft) thickness at their maximum in the outcrop. The bedsets are composed of structureless sandstone with small amounts of large-scale trough cross-bedded, tangential and sigmoidal cross-bedded sandstone and contains mudstone intraclast conglomerate along basal erosional scours. Locally, mud clasts are

up to 0.5 m (1.6 ft) long. In places, the upper part of these internal units comprises centimeter-scale alternations of sandstone/siltstone and mudstone layers. The paleocurrent measurements range from northeast (azimuth 43°) to southeast (azimuth 109°) direction suggesting that the channel flowed broadly eastward, rather than CD1, which flowed broadly to the north.

The structureless nature, large clasts, and internal scour surfaces suggests that channel deposit CD3 was deposited during intervals of extremely high-flow conditions (Wizevich, 1992) within a distributary channel. A lack of burrowing, compared to CD1, suggests that channel discharge was too high to allow any significant incursion of marine water. Channel deposits of CD3 are not recognized anywhere on the 2-D intermediate GPR grid. The outcrop thus intersects the western margin of a large, northeastward flowing channel deposit.

Channel Deposit 4

Channel deposit 4 is the uppermost unit and also lies at the top of SC7. Channel deposit 4 has an erosive basal bounding surface with moderate local relief and overlies all previously described channel deposits (Figure 7). Overall, CD4 is tabular, with significant increase in thickness toward the west (about 4.5 m [15 ft] interpreted from the GPR data). Element CD4 consists of a complex mixture of medium- and large-scale, trough cross-bedded sandstone, planar-tabular cross-bedded sandstone with some mudstone drapes on foresets, and sandstone containing convolute stratification. Grain size within CD4 is highly variable ranging from medium- to coarse-grained sandstone in fining- and coarsening-upward successions.

Paleocurrent directions reflect the depositional complexity of this uppermost element and ranges from a northeast (azimuth 60°) paleoflow on planar cross-beds to a southeast (azimuth 140°) paleoflow on trough cross-beds. These alternating current directions suggest tidal influence, probably related to the overall transgression that caps SC7 at the top of the Ferron clastic wedge. Poor exposure of CD4 in outcrops (due to erosion) made it difficult to determine the detailed bedding architecture and further interpretation has not been attempted.

DISCUSSION

The inclined bedsets deposited at Corbula Gulch are an excellent example of marine influenced point bars deposited within lower delta-plain distributary channels, and are quite different from the non-migratory, straight channels that are inferred to be typical of lower delta-plain distributary channels (e.g. Coleman and Prior, 1982). These channels were affected by seasonal and possibly longer-term changes in channel discharge, but show little evidence of tidal processes. The charac-

teristics of this point bar deposited in a lower delta plain differs from classical fluvial point bars, but also does not match well with standard models for distributary channels. The 3-D geometry of the inclined surfaces within the point bar indicates that they were formed by lateral and upstream migration (Figures 15A and B). The laterally accreting bedset surfaces show, in vertical section, perpendicular to flow, more linear to concave-upward shapes, with long asymptotic ends toward the channel axis (Figure 15A). This tendency of the inclined beds to follow the shape of the channel was related by Hopkins (1985) to the existence of "passive" point bars that plug the channel before abandonment. Probably the easternmost inclined bedset represents the initial phase of channel infilling and abandonment. Also, these concave-upward shapes are more linear and divergent in plan view (Figure 15C) compared to the arcuate pattern of the swell and ridge topography of other fluvial point bars (cf. Puigdefabregas and van Vliet, 1978; Gibling and Rust, 1993).

Compared to simple theoretical models of fluvial point bars (Bridge, 1984; Willis, 1989) the inclined bedsets at Corbula Gulch show a much more complex grain-size distribution than the theoretical fining-upward and downstream trend. Also, the inclined bed surfaces are concave upward and migrate both laterally and upstream, while theoretical model generally predict convex upward inclined surfaces, migrating laterally and downstream. Upstream migration of the point bars is not usually depicted in theoretical models of fluvial point bars (Willis, 1989). Other factors, such as marine influence, decrease in discharge and slope within distributary channels, may be required to generate more representative theoretical models of point-bar deposits associated with distributary channels.

The lithologic heterogeneities at Corbula Gulch are represented by mudstone drapes along inclined accretion surfaces, and by mudstone intraclast conglomerate along minor erosional surfaces separating the inclined beds. Quantification of 3-D distribution of the mudstone drapes is performed through geostatistical analysis of 3-D GPR amplitudes. These mudstones are not extensive parallel to the flow and are never longer than 15 m (49 ft). Initially longer mudstones are typically fragmented to smaller dimensions of 5 m (16 ft) as a consequence of erosional scour by overlying units. Along the downdip direction, the mudstones average 10 m (33 ft) long. Combining the 3-D architecture of point-bar deposits and the 3-D distribution of heterogeneities constitutes important input to reservoir flow simulation (e.g. Novakovic et al., 2002).

CONCLUSION

Point-bar deposits within lower delta-plain, high-sinuosity distributary channels are described and inter-

preted at Corbula Gulch, in the fluvio-deltaic Cretaceous Ferron Sandstone Member of the Mancos Shale. The paleoshoreline is located at 24 km (15 mi) north, and marine (*Teredolites*) and brackish water (*Skolithos*, *Arenicolites*, *Thalassinoides*) burrows are common within the delta-plain deposits and the mudstone/siltstone drapes at the tops of the inclined beds.

The grain-size distribution is more complex than the upward- and downstream-fining prediction from theoretical point-bar models.

The inclined bedset surfaces migrated laterally and upstream and show concave-upward shapes paralleling the channel. In horizontal section these inclined surfaces are linear and divergent, parallel to the channel cutbank. Present fluvial theoretical models do not predict these geometries and these geometries may be more characteristic of point bars formed within marine-influenced distributary channels (Bhattacharya et al., 2001).

The main radar facies characterizing the point-bar deposits in 3-D and 2-D GPR surveys are inclined, parallel or concave upward, continuous, high-amplitude reflections that truncate upward against the erosional surface of the overlying deposits and downlap downward onto the base of the channel.

The estimated minimum paleochannel bankfull width and mean depth are 150 m (492 ft) and 4 m (13 ft), respectively, but the upper part of the inclined beds is probably completely removed by erosion and thus we may be underestimating the dimensions of the inclined beds.

The main heterogeneities within the point-bar deposits at Corbula Gulch are shale drapes on the inclined accretion surfaces, and mudstone intraclast conglomerate along basal erosional surfaces of the inclined beds. These high clay content layers were originally longer parallel to the flow (15 m [49 ft]) but are now discontinuous (< 5 m [16 ft]) because of deep erosion by the overlying units. Perpendicular to the flow (downdip the inclined beds) the mudstone and mudstone intraclast conglomerate are more continuous, reaching about 10 m (33 ft) in length. This detailed distribution of the heterogeneities within a reservoir analog interpreted from GPR data is important to predict flow behaviour.

ACKNOWLEDGMENTS

The research leading to this paper was funded primarily by the U.S. Department of Energy under Contract DE-FG03-96ER14596 with auxiliary support from the University of Texas at Dallas GPR Consortium. The interpretation of the migrated data was done using the PC-based seismic interpretation software WinPics of Kernek Technologies Ltd. The geostatistical analysis was done with the Geostatistical Software Library (GSLIB) programs. The permeability measurements were collected and analyzed by Steve Snelgrove and

Craig Forster from the University of Utah. An earlier version of this paper benefited from reviews by John Bridge. This paper is contribution number 996 from the Geosciences Department at the University of Texas at Dallas.

REFERENCES CITED

- Alexander, J., J. S. Bridge, M. R. Leeder, R. E. L. Collier, and R. L. Gawthorpe, 1994, Holocene meander-belt evolution in an active extensional basin, southwestern Montana: *Journal of Sedimentologic Research*, v. B64, p. 542-559.
- Allen, J. R. L., 1964, Studies in fluvial sedimentation: six cyclothems from the Lower Old Red Sandstone, Anglo-Welsh basin: *Sedimentology*, v. 3, p. 163-198.
- 1970, Studies in fluvial sedimentation: a comparison of finning upwards cyclothems with special reference to coarse-member composition and interpretation: *Journal of Sedimentary Petrology*, v. 40, p. 298-323.
- Annan, A. P., S. W. Cosway, and J. D. Redman, 1991, Water table detection with ground-penetrating radar (abs.): SEG Annual International Meeting and Exposition, Program with Abstracts, E/G1.4, p. 494-497.
- Baker, P. L., and U. Monash, 1991, Fluid, lithology, geometry, and permeability information from ground-penetrating radar for some petroleum industry applications: Society of Petroleum Engineer, paper SPE 22976, p. 277-286.
- Barton, M. D., 1994, Outcrop characterization of architecture and permeability structure in fluvial-deltaic sandstones, Cretaceous Ferron sandstone, Utah: Ph.D. dissertation, University of Texas, Austin, Texas, 260 p.
- Beres, M., A. Green, P. Huggenberger, and H. Horstmeyer, 1995, Mapping the architecture of glaciofluvial sediments with three dimensional georadar: *Geology*, v. 23, p. 1087-1090.
- Bhattacharya, J. P., R. M. Corbeanu, and C. Olariu, 2001, Downstream causes of avulsion in distributary channels, as seen in Cretaceous sandstones of Central Utah (abs): 7th International Conference on Fluvial Sedimentology, program and abstracts, Open-File Report 60, Conservation and Survey Division, Institute of Agriculture and Natural Resources, University of Nebraska-Lincoln, p.59.
- Bluck, B. G., 1971, Sedimentation in the meandering River Endrick: *Scottish Journal of Geology*, v. 7, p. 93-138.
- Bridge, J. S., 1984, Flow and sedimentary processes in river bends: comparison of field observation and theory, in M. Elliot, ed., *River meandering: Proceedings Rivers '83*, American Society of Civil Engineers, p. 857-872.
- 1985, Paleochannel patterns inferred from alluvial deposits: a critical review: *Journal of Sedimentary Petrology*, v. 55, p. 579-589.
- 1993, Description and interpretation of fluvial deposits: a critical perspective: *Sedimentology*, v. 42, p. 801-810.
- Bridge, J. S., and J. Jarvis, 1976, Flow and sedimentary processes in the meandering River South Esk, Glen Clova, Scotland: *Earth Surface Processes*, v. 2, p. 401-416.
- Bridge, J. S., J. Alexander, R. E. L. Collier, R. L. Gawthorpe, and J. Jarvis, 1995, Ground-penetrating radar and coring used to study the large-scale structure of point-bar deposits in three dimensions: *Sedimentology*, v. 42, p. 839-852.
- Bridge, J. S., R. E. L. Collier, and J. Alexander, 1998, Large-scale structures of Calamus River deposits (Nebraska, U.S.A.) revealed using ground-penetrating radar: *Sedimentology*, v. 45, p. 977-986.
- Bristow, C. S., 1993, Sedimentary structures exposed in bar tops in the Brahmaputra River, Bangladesh, in J. L. Best and C. S. Bristow, eds., *Braided rivers: Geological Society of London Special Publication 75*, p. 277-289.
- 1995, Internal geometry of ancient tidal bedforms revealed using ground penetrating radar, in B. W. Flemming and A. Bartholoma, eds., *Tidal signatures in modern and ancient sediments: International Association of Sedimentologists Special Publications*, v. 24, p. 313-328.
- Bristow, C. S., P. N. Chroston, and S. D. Bailey, 2000, The structure and development of foredunes on a locally prograding coast: insights from ground-penetrating radar surveys, Norfolk, UK: *Sedimentology*, v. 47, p. 923-944.
- Bromley, R. G., G. Pemberton, and R. A. Rahmani, 1984, A Cretaceous woodground: the *teredolites* ichnofacies: *Journal of Paleontology*, v. 58, p. 488-498.
- Brown, A. R., 1996, Interpretation of three-dimensional seismic data: AAPG Memoir 42, 4th ed., 444 p.
- Cherven, V. B., 1978, Fluvial and deltaic facies in the Sentinel Butte Formation, central Eilliston basin: *Journal Sedimentary Petrology*, v. 48, p. 159-170.
- Coleman, J. M., and D. B. Prior, 1982, Deltaic environments of deposition, in P.A. Scholle and D. Spearing, eds., *Sandstone depositional environments: AAPG Memoir 31*, p. 139-178.
- Corbeanu, R. M., K. Soegaard, R. B. Szerbiak, J. B. Thurmond, G. A. McMechan, D. Wang, S. H. Snelgrove, C. B. Forster, and A. Menitove, 2001,

- Detailed internal architecture of a fluvial channel sandstone determined from outcrop, cores and 3-D ground-penetrating radar: example from the Mid-Cretaceous Ferron Sandstone, east-central Utah: *AAPG Bulletin*, v. 85, p. 1583-1608.
- Cotter, E., 1975, Late Cretaceous sedimentation in a low energy coastal zone: the Ferron Sandstone of Utah: *Journal of Sedimentary Petrology*, v. 45, p. 669-685.
- Davis, J. L., and A. P. Annan, 1989, Ground-penetrating radar for high resolution mapping of soil and rock stratigraphy: *Geophysical Prospecting*, v. 37, p. 531-551.
- Deutsch, C. V., and A. G. Journel, 1998, *GSLIB geostatistical software library and user's guide*: Oxford, Oxford University Press, 340 p.
- Dreyer, T., 1993, Geometry and facies of large-scale flow units in fluvial-dominated fan-delta-front sequences, in M. Ashton, ed., *Advances in reservoir geology*: Geological Society Special Publication 69, p. 135-174.
- Elliott, T., 1976, The morphology, magnitude and regime of a Carboniferous fluvial-distributary channel: *Journal of Sedimentary Petrology*, v. 46, p. 70-76.
- Ethridge, F. G., and S. A. Schumm, 1978, Reconstructing paleochannel morphologic and flow characteristics: methodology, limitations, and assessment, in A. D. Miall, ed., *Fluvial sedimentology*: Canadian Society of Petroleum Geology Memoir 5, p. 703-721.
- Falkner, A., and C. R. Fielding, 1993, Quantitative facies analysis of coal-bearing sequences in the Bowen Basin, Australia: applications to reservoir description, in S. S. Flint and I. D. Bryant, eds., *The geological modeling of hydrocarbon reservoirs and outcrop analogs*: International Association of Sedimentologists Special Publication 15, p. 81-89.
- Fielding, C. R., 1984, Upper delta plain lacustrine and fluvial-lacustrine facies from the Westphalian of the Durham coalfield, NE England: *Sedimentology*, v. 31, p. 547-567.
- Flint, S. S., and D. Bryant, eds., 1993, *The geological modeling of hydrocarbon reservoirs and outcrop analogs*: International Association of Sedimentologists Special Publication 15, 269 p.
- Gardner, M. H., 1992, Sequence stratigraphy of the Ferron Sandstone, east-central Utah, in N. Tyler, M. D. Barton, and R. S. Fisher, eds., *Architecture and permeability structure of fluvial-deltaic sandstones: a field guide to selected outcrops of the Ferron Sandstone, east-central Utah*: Austin, University of Texas, Bureau of Economic Geology Guidebook, p. 1-12.
- 1995, Tectonic and eustatic controls on the stratal architecture of mid-Cretaceous stratigraphic sequences, central western interior foreland basin of North America, in S. L. Dorobek and G. M. Ross, eds., *Stratigraphic evolution of foreland basins*: Society for Sedimentary Geology (SEPM) Special Publication 52, p. 243-281.
- Garrison, J. R., Jr., T. C. V. van den Bergh, C. E. F. Barker, and D. E. Tabet, 1997, Depositional sequence stratigraphy and architecture of the Cretaceous Ferron Sandstone: implications for coal and coalbed methane resources - a field excursion, in P. K. Link and B. J. Kowallis, eds., *Mesozoic to recent geology of Utah*: Provo, Brigham Young University Geology Studies v. 42, pt. 2, p. 155-202.
- Gawthorpe, R. L., R. E. L. Collier, J. Alexander, J. S. Bridge, and M. R. Leeder, 1993, Ground-penetrating radar: application to sandbody geometry and heterogeneity studies, in C. P. North and D. J. Prosser, eds., *Characterization of fluvial and aeolian reservoirs*: Geological Society Special Publication 73, p. 421-432.
- Gibling, M. R., and B. R. Rust, 1993, Alluvial ridge-and swale topography: a case study from the Morien Group of Atlantic Canada, in M. Marzo and C. Puygdefabregas, eds., *Alluvial sedimentation*: International Association of Sedimentologists Special Publications 17, p. 133-150.
- Hale, L. A., 1972, Depositional history of the Ferron Formation, central Utah, in J. L. Baer, ed., *Plateau-basin and range transition zone*: Utah Geological Association Publication 2, p. 115-138.
- Hammon, W. S., III, X. Zeng, R. M. Corbeau, and G. A. McMechan, 2002, Estimation of the spatial distribution of fluid permeability from surface and tomographic GPR data and core, with a 2-D example from the Ferron Sandstone, Utah: *Geophysics*, v. 67, p. 1505-1515.
- Hobday, D. K., 1978, Fluvial deposits of the Ecca and Beaufort Groups in the eastern Karoo Basin, Southern Africa, in A. D. Miall, ed., *Fluvial sedimentology*: Canadian Society of Petroleum Geology Memoir 5, p. 413-429.
- Hopkins, J. C., 1985, Channel-fill deposits formed by aggradation in deeply scoured, superimposed distributaries of the Lower Kootenai Formation (Cretaceous): *Journal of Sedimentary Petrology*, v. 55, p. 42-52.
- Hornung, J., and T. Aigner, 2000, Integration of outcrop sedimentology, petrophysics and georadar for enhanced 3-D reservoir-characterization of fluvial sandstones (Triassic, Germany): Geological Society of America International Meeting, Abstracts with Program, A-80.
- Jackson, R. G., II, 1976, Depositional model of point bars in the lower Wabash River: *Journal of Sedimentary*

- Petrology, v. 46, p. 579-594.
- 1978, Preliminary evaluation of lithofacies models for meandering alluvial streams, *in* A. D. Miall, ed., *Fluvial sedimentology: Canadian Society of Petroleum Geologists Memoir 5*, p. 543-576.
- 1981, Sedimentology of muddy fine-grained channel deposits in meandering streams of the American Middle West: *Journal of Sedimentary Petrology*, v. 51, p. 1169-1192.
- Jordan, D. W., and W. A. Pryor, 1992, Hierarchical levels of heterogeneity in a Mississippi River meander belt and application to reservoir systems: *AAPG Bulletin*, v. 76, p. 1601-1624.
- Knight, R. J., and A. Nur, 1987, The dielectric constant of sandstones, 60kHz to 4MHz: *Geophysics*, v. 52, p. 644-654.
- Lowry, P., and T. Jacobsen, 1993, Sedimentological and reservoir characteristics of a fluvial-dominated delta-front sequence: Ferron Sandstone Member (Turonian), east-central Utah, USA, *in* M. Ashton, ed., *Advances in reservoir geology: Geological Society Special Publication 69*, p. 81-103.
- Miall, A. D., and C. E. Turner-Peterson, 1989, Variations in fluvial style in the Westwater Canyon Member, Morrison Formation (Jurassic), San Juan Basin, Colorado Plateau: *Sedimentary Geology*, v. 63, p. 21-60.
- McMechan, G. A., G. C. Gaynor, and R. B. Szerbiak, 1997, Use of ground-penetrating radar for 3-D sedimentological characterization of clastic reservoir analogs: *Geophysics*, v. 62, p. 786-796.
- Nelson, B. W., 1970, Hydrography, sediment dispersal and recent historical development of the Po River delta, Italy, *in* J. P. Morgan and R. H. Shaver, eds., *Deltaic sedimentation, modern and ancient: Society for Sedimentary Geology (SEPM) Special Publication 15*, p. 152-184.
- Nio, S. D., and C. S. Yang, 1991, Diagnostic attributes of clastic tidal deposits: a review, *in* D. G. Smith, G. E. Reinson, B. A. Zaitlin, and R. A. Rahmani, eds., *Clastic tidal sedimentology: Canadian Society of Petroleum Geologists Memoir 16*, p. 3-28.
- Novakovic, D., C. D. White, R. M. Corbeanu, W. S. Hammon III, J. P. Bhattacharya, and G. A. McMechan, 2002, Effects of shales in fluvial-deltaic deposits: ground-penetrating radar, outcrop observations, geostatistics and three-dimensional flow modeling for the Ferron Sandstone, Utah: *Mathematical Geology*, v. 34, p. 857-893.
- Pemberton, S. G., J. A. MacEachern, and R. W. Frey, 1992, Trace fossil facies models: environmental and allostratigraphic significance, *in* R. G. Walker and N. P. James, eds., *Facies models response to sea level change: Geological Association of Canada Geotext 1*, p. 47-72.
- Plint, A. G., 1983, Facies, environments and sedimentary cycles in the Middle Eocene, Bracklesham Formation of the Hampshire Basin: evidence for global sea-level changes: *Sedimentology*, v. 30, p. 625-653.
- Puigdefabregas, C., and A. van Vliet, 1978, Meandering stream deposits from the Tertiary of the Southern Pyrenees, *in* A. D. Miall, ed., *Fluvial sedimentology: Canadian Society of Petroleum Geologists Memoir 5*, p. 469-485.
- Rea, J., and R. Knight, 1998, Geostatistical analysis of ground-penetrating radar data: a means of describing spatial variation in the subsurface: *Water Resources Research*, v. 34, p. 329-339.
- Robertson, J. D., and H. H. Nogami, 1984, Complex seismic trace analysis of thin beds: *Geophysics*, v. 49, p. 344-352.
- Ryer, T. A., 1981, Deltaic coals of Ferron Sandstone Member of Mancos Shale: predictive model for Cretaceous coal-bearing strata of Western Interior: *AAPG Bulletin*, v. 65, p. 2323-2340.
- 1991, Stratigraphy, facies and depositional history of the Ferron Sandstone in the Canyon of Muddy Creek, east-central Utah, *in* T. C. Chidsey, Jr., ed., *Geology of east-central Utah: Utah Geological Association Publication 19*, p. 45-54.
- Ryer, T. A., and P. B. Anderson, 1995, Parasequence sets, parasequences, facies distributions, and depositional history of the Upper Cretaceous Ferron deltaic clastic wedge, central Utah (abs.): *AAPG Bulletin*, v. 79, p. 924.
- Smith, D. G., 1987, Meandering river lithofacies models: modern and ancient examples compared, *in* Recent developments in fluvial sedimentology: Society for Sedimentary Geology (SEPM) Special Publication, Proceedings of 3rd International Fluvial Sedimentology Conference, Fort Collins, Colorado, August 1985.
- Stephens, M., 1994, Architectural element analysis within the Kayenta Formation (Lower Jurassic) using ground-probing radar and sedimentological profiling, southwestern Colorado: *Sedimentary Geology*, v. 90, p.179-211.
- Szerbiak, R. B., G. A. McMechan, R. M. Corbeanu, C. B. Forster, and S. H. Snelgrove, 2001, 3-D characterization of a clastic reservoir analog: from 3-D GPR to a 3-D fluid permeability model: *Geophysics*, v. 66, p. 1026-1037.
- Tanner, M. T., F. Koehler, and R. E. Sheriff, 1979, Complex seismic trace analysis: *Geophysics*, v. 44, p. 1041-1063.

- Thomas, R. G., D. G. Smith, J. M. Wood, J. Visser, E. A. Calverley-Range, and E. H. Koster, 1987, Inclined heterolithic stratification - terminology, description, interpretation and significance: *Sedimentary Geology*, v. 53, p. 123-179.
- Vail, P. R., 1987, Seismic stratigraphic interpretation procedure, *in* A. W. Bally, ed., *Atlas of seismic stratigraphy: AAPG Studies in Geology* 27, p. 1-10.
- Van Wagoner, J. C., R. M. Mitchum, K. M. Campion, and V. D. Rahmanian, 1990, Siliciclastic sequence stratigraphy in well logs, cores and outcrops: concepts for high-resolution correlation of time and facies: *AAPG Methods in Exploration* 7, 55 p.
- Willis, B J., 1989, Paleochannel reconstructions from point bar deposits: a three-dimensional perspective: *Sedimentology*, v. 36, p. 757-766.
- 1993, Interpretation of bedding geometry within ancient point-bar deposits, *in* M. Marzo and C. Puigdefabregas, eds., *Alluvial sedimentation: International Association of Sedimentologists Special Publication* 17, p. 101-114.
- Wizevich, M. C., 1992, Pennsylvanian quartzose sandstones of the Lee Formation: fluvial interpretation based on lateral profile analysis: *Sedimentary Geology*, v. 78, p. 1-47.
- Xu, X., 2000, Three-dimensional virtual geology: photo-realistic outcrops, and their acquisition, visualization and analysis: Ph.D. dissertation, University of Texas at Dallas, Dallas, 400 p.